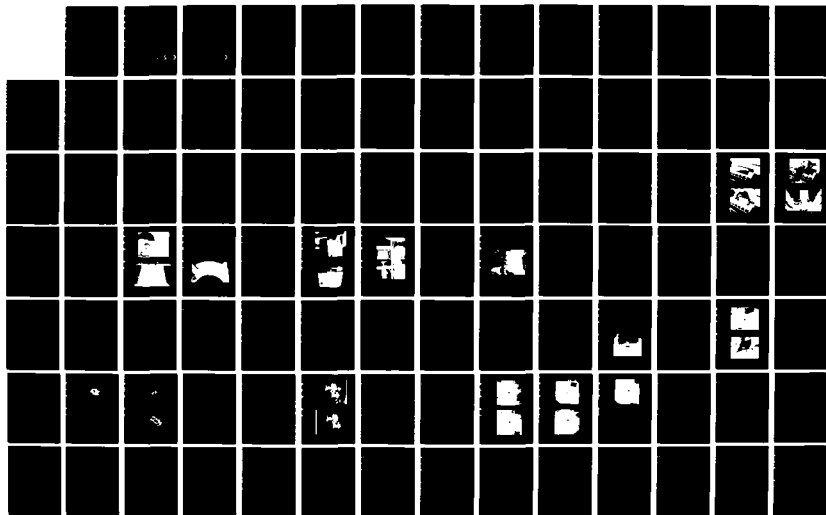


AD-A164 110

THE EFFECTS OF THROUGH THE THICKNESS DELAMINATIONS ON  
CURVED COMPOSITE PANELS(U) AIR FORCE INST OF TECH  
WRIGHT-PATTERSON AFB OH SCHOOL OF ENGI B A HORBAN  
UNCLASSIFIED DEC 85 AFIT/GAE/AA/85D-8 F/G 13/13

1/2

NL





MICROCOPY RESOLUTION TEST CHART  
NATIONAL BUREAU OF STANDARDS-1963-A

1

AD-A164 110



THE EFFECTS OF THROUGH THE THICKNESS  
DELAMINATIONS ON CURVED COMPOSITE PANELS

THESIS

Blaise A. Horban  
Captain USAF  
AFIT/GAE/AA/85D-8

DISTRIBUTION STATEMENT A

Approved for public release  
Distribution Unlimited

DEPARTMENT OF THE AIR FORCE  
AIR UNIVERSITY

**AIR FORCE INSTITUTE OF TECHNOLOGY**

Wright-Patterson Air Force Base, Ohio

DTIC  
ELECTE  
FEB 13 1986

B

DTIC FILE COPY

86 2 13

AFIT/GAE/AA/85D-8

THE EFFECTS OF THROUGH THE THICKNESS  
DELAMINATIONS ON CURVED COMPOSITE PANELS

THESIS

Blaise A. Horban  
Captain USAF  
AFIT/GAE/AA/85D-8

DTIC  
ELECTE  
FEB 13 1986  
S D  
B

Approved for public release; distribution unlimited.

AFIT/GAE/AA/85D-8

THE EFFECTS OF THROUGH THE THICKNESS  
DELAMINATIONS ON CURVED COMPOSITE PANELS

THESIS

Presented to the Faculty of the School of Engineering  
of the Air Force Institute of Technology  
Air University  
in Partial Fulfillment of the  
Requirements for the Degree of  
Master of Science

by

Blaise A. Horban  
Captain, USAF

December 1985

Approved for public release; distribution unlimited.

## Acknowledgements

I wish to express my sincere gratitude to Dr. Anthony Palazotto for his patience and expert guidance in completing this thesis.

I would also like to thank the Flight Dynamics Laboratory, in particular Mr. Jack Smith and Mr. Harold Croop, for the support and funding for this research. I would like to thank Debra Olivaria who also provided her expertise in accomplishing parts of this thesis. I would especially like to thank Mr. Gene Maddux who spent countless hours explaining many of the principles and theory behind the examination techniques to me.

In addition, I greatly appreciate the editing and patience of Lynne Pompetti. Finally, I would like to thank all my friends and family who supported and encouraged me throughout this thesis.



Accession For	
NTIS GNARI	<input checked="checked" type="checkbox"/>
NTIS TAP	<input type="checkbox"/>
Unannounced	<input type="checkbox"/>
Justification	
Distribution/	
Availability Group	
Post	Special
A-1	

## Table of Contents

	<u>Page</u>
Acknowledgments . . . . .	ii
List of Symbols . . . . .	v
List of Figures . . . . .	vii
List of Tables . . . . .	x
Abstract . . . . .	xi
I. Introduction . . . . .	1
Background . . . . .	1
Purpose . . . . .	3
Scope . . . . .	4
II. Theory . . . . .	8
Bifurcation Buckling . . . . .	8
Classical Lamination Theory . . . . .	8
Delamination and Panel Buckling States . . . . .	14
STAGSC-1 Theory . . . . .	18
Experimental Techniques to Evaluate Defect Size and Location in Composites . . . . .	19
III. Manufacturing and Experimental Procedure . . . . .	24
Panel Manufacturing . . . . .	24
Experimental Set-Up . . . . .	29
Test Procedure . . . . .	35

	<u>Page</u>
IV. Results and Discussion . . . . .	38
Panel Identification . . . . .	38
Data Output . . . . .	39
Analytical/Experimental Comparison . . . . .	46
Buckling Patterns . . . . .	49
X-ray/ C-Scan Results . . . . .	55
Stereo X-ray . . . . .	59
Deply Technique . . . . .	60
Equivalent Delamination . . . . .	63
Verification Testing . . . . .	69
V. Conclusions . . . . .	72
Buckling Instability . . . . .	72
Experimental Procedures . . . . .	73
Bibliography . . . . .	75
Appendix A: Stiffness and Effective Laminate Properties . . . . .	78
Appendix B: Analytical Non-Dimensionalized Values . . . . .	81
Appendix C: Test Data . . . . .	85
Appendix D: Actual Delaminated Area for Stereo X-ray Panels . . . . .	88
Appendix E: Actual Delaminated Area for Deply Panels . . . . .	89
Vita . . . . .	90



### List of Symbols

$E_1$	Longitudinal Modulus of Elasticity
$E_2$	Transverse Modulus of Elasticity
$G_{12}$	Shear Modulus
$u, v, w$	Displacements in x, y, z directions, respectively
$w_{,x}$	Comma denotes partial differentiation
$t$	Panel Thickness
$R$	Panel Radius of Curvature
$C$	Panel Chord
$L$	Panel Length
$x, y, w$	Structural Coordinate Directions
$\beta$	Stereo X-ray Incidence Angle
$Q_{ij}$	Transformed Reduced Stiffness
$A_{ij}$	Extensional Stiffness
$B_{ij}$	Coupling Stiffness
$D_{ij}$	Bending Stiffness
$z$	Distance From Panel Mid-surface

$K$	Curvature
$N_x, N_y, N_{xy}$	Force Resultants
$M_x, M_y, M_{xy}$	Moment Resultants
$a$	Delamination Radius
$\rho$	Ratio of Bending Strain Versus Membrane Strain
$\theta$	Ply Orientation
$\nu$	Poisons' Ratio
$\tilde{a}$	Non-dimensionalized Delamination Radius
$\tilde{G} \tilde{a}^4$	Non-dimensionalized Energy-Release Rate
$\sigma$	Normal Stress
$\tau$	Shear Stress
$\epsilon$	Direct Strain
$\gamma$	Shear Strain

## List of Figures

<u>Figure</u>	<u>Page</u>
1. Panel Geometry . . . . .	6
2. Cross Section of Panel Thickness at Delamination Locations . . . .	7
3. Panel End-Shortening . . . . .	9
4. Positive Force and Moment Directions . . . . .	12
5. Stereo X-ray Arrangement . . . . .	21
6. Layup of Four Small Panels in One Large Mold . . . . .	26
7. Mylar Template Used to Place Delamination Causing Insert . . . .	26
8. Large Panel Sealed In Nylon Bag . . . . .	27
9. Four Large Molds in Autoclave . . . . .	27
10. Length Dimension Being Cut Using Special Fixture . . . . .	30
11. Steel Plates for Top and Bottom Boundary Conditions . . . . .	30
12. Panel In Test Fixture Showing Steel Wedges . . . . .	31
13. Knife Edge with "O" Ring . . . . .	33
14. Knife Edge Installed In Vertical Support . . . . .	33
15. Complete Experimental Setup . . . . .	34
16. Outer Surface LVDTs . . . . .	36
17. Cross Section of Panel Q12 at Delamination Locations . . . . .	40

	<u>Page</u>
18. Cross Section of Panel Q22 at Delamination Locations . . . . .	41
19. Panel End-Shortening . . . . .	43
20. Strain Reversal . . . . .	43
21. Panel Q123T End-Shortening . . . . .	44
22. Panel Q123T Strain Reversal . . . . .	45
23. Knockdown Factor vs Delaminated Area at Buckling (Panels with Teflon Inserts) . . . . .	48
24. End-Shortening vs Delaminated Area at Buckling (Panels with Teflon Inserts) . . . . .	48
25. Panel Deformation as Load is Applied (Vertical Plane of Symmetry) . . . . .	50
26. Panel Deformation as Load is Applied (Horizontal Plane of Symmetry) . . . . .	50
27. Panel Buckling Shape (Horizontal Plane of Symmetry) . . . . .	52
28. Q122T in its Buckled Shape . . . . .	52
29. Local Buckling on the Outer Surface . . . . .	53
30. Asymmetrical Buckling Pattern of Panel Q131 . . . . .	54
31. Asymmetrical Buckling Pattern of Panel Q121 . . . . .	54
32. X-ray of Completely Delaminated Panel . . . . .	57
33. X-ray of Partially Delaminated Panel . . . . .	57
34. X-ray of Q133 After 1/2 Hour Penetration . . . . .	58

	<u>Page</u>
35. X-ray of Q133 After One Hour Penetration . . . . .	58
36. Normal X-ray of Panel Q241 . . . . .	61
37. Interpretation of Stereo X-ray of Panel Q241 . . . . .	61
38. Knockdown Factor vs Total Actual Delaminated Area (Stereo X-ray Panels) . . . . .	62
39a. Delamination Between Plies Six and Seven ( $-45^{\circ}$ Ply) . . . . .	64
39b. Delamination Between Plies Five and Six ( $+45^{\circ}$ Ply) . . . . .	64
39c. Delamination Between Plies Four and Five ( $90^{\circ}$ Ply) . . . . .	65
39d. Delamination Between Plies Three and Four ( $90^{\circ}$ Ply) . . . . .	65
39e. Delamination Between Plies Two and Three ( $+45^{\circ}$ PLy) . . . . .	66
40. Knockdown Factor vs Total Actual Delaminated Area at Buckle ( Deply Panels) . . . . .	66
41. Knockdown Factor vs Total Actual Delaminated Area (Deply and Stereo X-ray Panels) . . . . .	68
42. End-Shortening vs Total Actual Delaminated Area ( Deply and Stereo X-ray Panels) . . . . .	69

## List of Tables

<u>Table</u>	<u>Page</u>
I. Code Representation For Panels Incorporated In Study . . . . .	38
II. Total Delamination Area In Deply and Stereo X-ray Panels . . . . .	67

Abstract

The buckling loads of 8-ply AS4/3501-6 graphite/epoxy delaminated cylindrical panels were determined experimentally. The delaminations fabricated into the laminate, with mylar and teflon inserts, were indicative of low velocity projectile impact damage. The mylar and teflon inserts caused partial and total delaminations, respectively. Two types of delaminations were used; namely, eccentric, off mid-surface, and mid-surface. The eccentric delaminations were placed progressively through the thickness of the laminate. STAGSC-1 finite element computer code results for undelaminated composite panels were compared to the experimental results to obtain a percent strength degradation.

The experimental testing was accomplished by the Air Force Flight Dynamics Laboratory. The test device provided boundary conditions of clamped top and bottom edges and simply supported vertical sides.

Two destructive techniques, stereo x-ray and deply, were used to determine the total delaminated areas and locations. Based in part on these results, one equivalent delamination was obtained corresponding to the total area of the multiple partial delaminations. The panels with multiple delaminations were found to be approximately 5 % weaker than a single delaminated area of the same total size.

# THE EFFECTS OF THROUGH THE THICKNESS DELAMINATIONS ON CURVED COMPOSITE PANELS

## I. Introduction

### Background

Composite materials are becoming increasingly popular for use in structures and applications where weight is critical. The United States Air Force is particularly interested in these materials for aircraft use. Added weight from aluminum or steel structures cause a like reduction in payload carrying capacity. Therefore, many new aircraft structures have incorporated advanced composites in their construction to take advantage of its high strength-to-weight ratios. Examples of this structural benefit can be cited in the McDonnell Douglas F-15 Eagle, the General Dynamics F-16 Falcon, and the Grumman, experimental forward swept wing, X-29.

The ever increasing use of composites has shown that problems exist which are not comparable to isotropic materials. One such problem, and the



subject of this thesis, is delaminations present within the laminate acted upon by compressive loading. This problem has recently received attention in order to predict the behavior of the laminate. The delaminations originate from many different sources. The type of delamination this thesis examines is similar to the delamination caused by a low velocity projectile impact which is characterized by sub-surface delaminations with little or no externally visible damage [1,2,3].

Several attempts have been made to describe the failure mechanisms of composite panel buckling with delaminations present. Two such attempts [4,5] used one-dimensional analytical models to predict delamination buckling loads. Later, Chai and Babcock [6] used a two-dimensional model to predict the loss of compressive strength due to a delamination brought about by a transverse impact. Shivakumar and Whitcomb [7], developed Rayleigh-Ritz and finite element methods to determine the bifurcation buckling of an elliptical delamination embedded near the surface of a thick quasi-isotropic laminate under compressive loading.

Fei and Yin [8] analyzed a circular delamination in a thin circular flat plate using the Von Karmen nonlinear plate equations. Their results indicate that a panel with a given delamination, under pure compression, will buckle while a panel loaded in such a fashion that the delamination undergoes both

compression and bending will experience buckling, snap-through (separation of the delaminated layer from the main body of the plate), and catastrophic failure if the load is sufficient to attain the critical value for growth of the delamination. Experimental work has been done [9] with a delamination located in the center of a cylindrical composite panel which verified, under certain geometric conditions, the usefulness of the Fei and Yin equations even for a curved surface.

Wilken's [10] initially developed a formulation to experimentally compare the buckling load of curved composite panels. The critical expression is referred to as the percent knockdown factor;

$$\text{Knockdown Factor} = \left( 1 - \frac{\text{experimental buckling load}}{\text{theoretical buckling load}} \right) \times 100$$

It indicates the decrease in the experimental buckling loads as compared to analytical values. This knockdown factor proved useful in Seifert's work [9].

### Purpose

The purpose of this research is to experimentally determine the buckling loads of curved composite panels with differing amounts of delamination present. These delaminations are indicative of the damage caused by low velocity projectile impact. The experimental panels have the

delaminations, in the form which would occur if the panels were impacted [4,5], fabricated into them using a delamination causing insert. Two types of insert material were used namely, mylar and teflon. These two were chosen based on previous work [3,9] and the types of delaminations needed. The mylar inserts cause only partial delaminations while the teflon inserts cause a complete or total delamination.

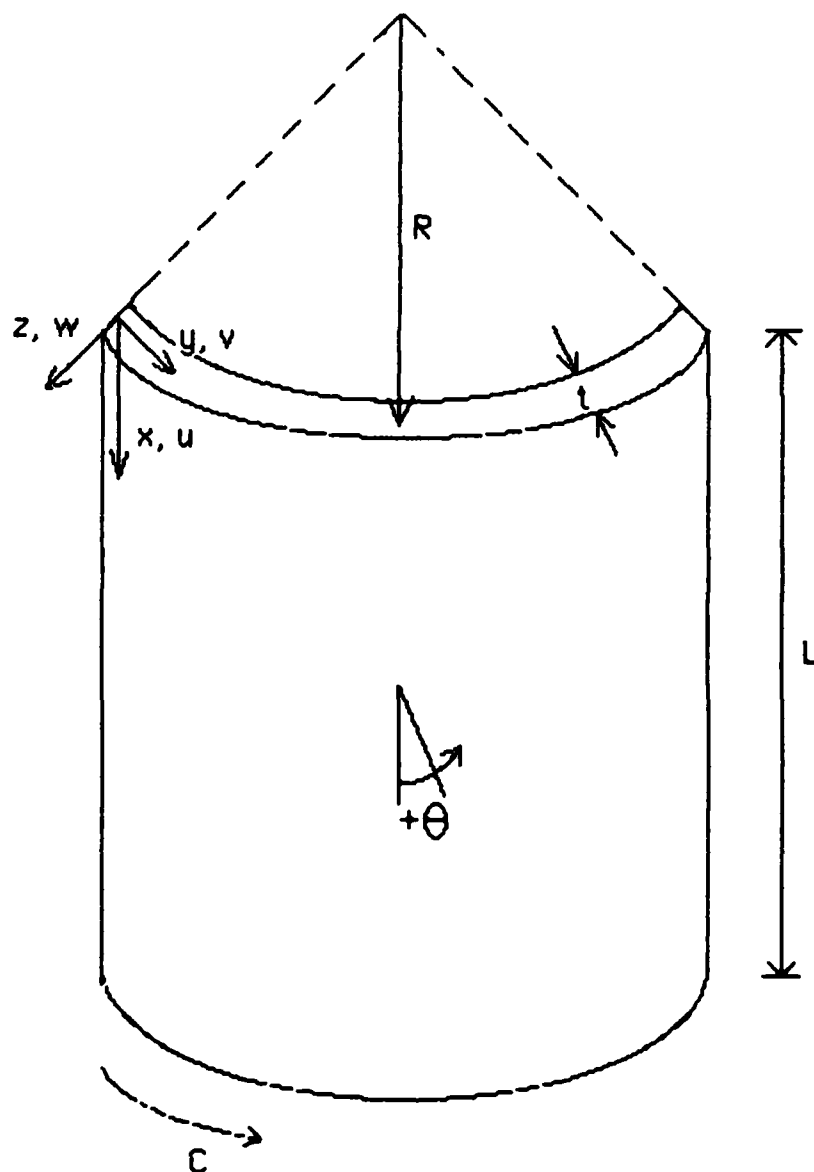
The linear bifurcation load calculated through the use of the STAGSC-1 Finite Element Computer Code is used as an upper bound for the buckling loads of the panels. The panels with teflon inserts form an upper bound for the panels with single mylar inserts which cause only partial delaminations. A second objective demonstrates an ability to examine panels after buckling with fabricated partial delaminations present using two destructive examination techniques. From these results an equivalent single delamination for the through the thickness partial delaminations is obtained. The data from this thesis will broaden the understanding of the buckling phenomenon in composite structures and post failure examination techniques.

### Scope

The experimental panels have a ply layup of  $(0/-45/+45/90)_s$  and dimensions of 12 in. X 12 in. (Fig. 1). Mylar and teflon are the two

different circular delamination causing inserts incorporated. Mylar causes only partial delaminations and teflon causes total delaminations. The delamination diameters consisted of 0 inch (no delamination), two inch, three inch, and four inch. The mylar inserts where placed progressively through the thickness beginning between plies six and seven. The teflon inserts were placed eccentrically, (see Fig. 2) in order to represent the effect of initial damage brought about by a projectile impact. A total of 56 eight ply graphite/epoxy panels where tested with four panels of each delamination configuration. All delamination causing inserts where placed at the geometric center of the panels.

The boundary conditions incorporated in the experimental test device are a clamped top edge ( $u = v = w = w_{,x} = 0$ ), clamped bottom edge ( $u = \text{free}$ ,  $v = w = w_{,x} = 0$ ), and simply supported on the vertical sides ( $u = v = w_{,y} = \text{free}$ ,  $w = w_{,x} = 0$ ). Fig. 1 shows the panel axis system.



$x, y, z$  = structural coordinates  
 $u, v, w$  = displacements  
 $t$  = thickness  
 $R$  = radius of curvature  
 $L$  = length  
 $\theta$  = ply orientation  
 $C$  = chord

Fig. 1. Panel Geometry

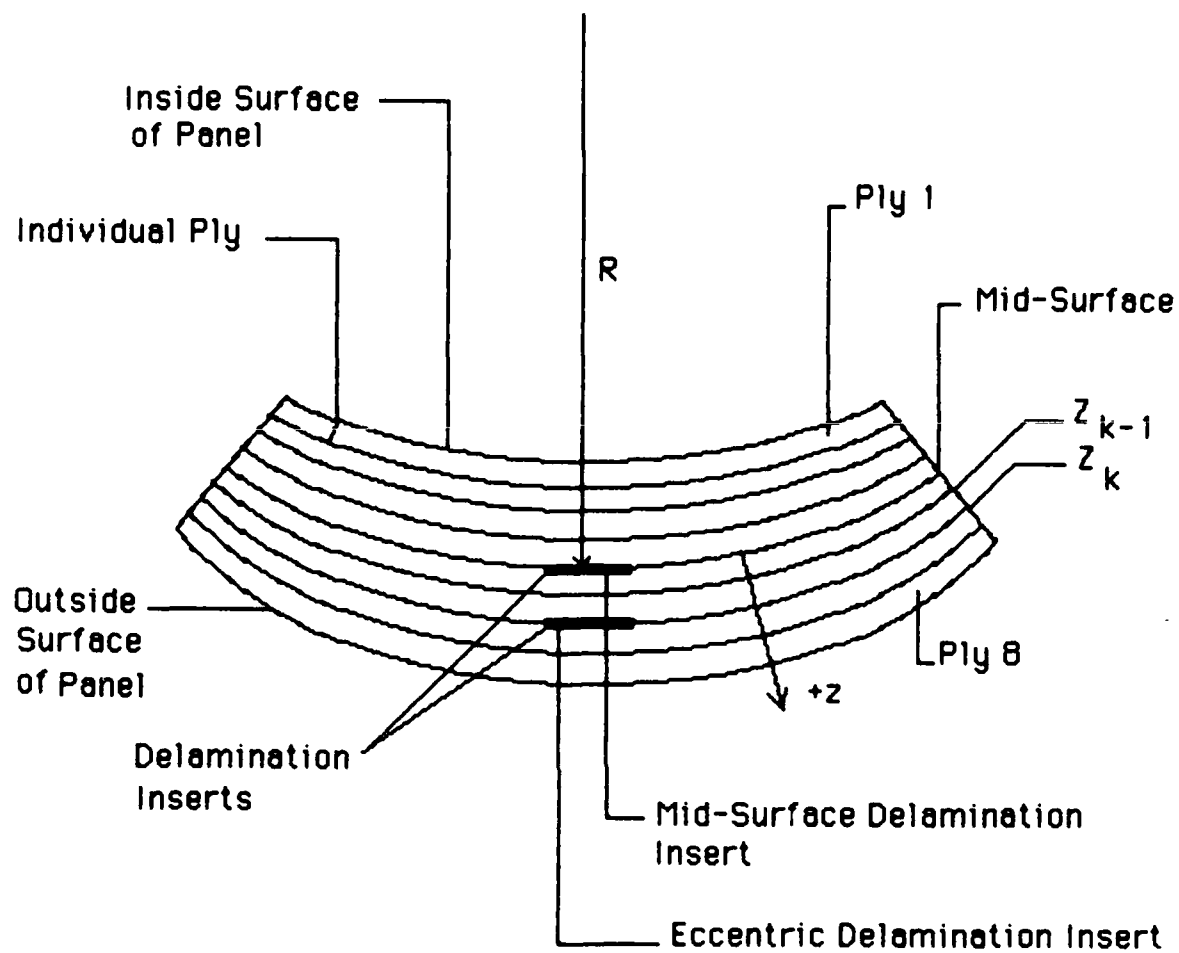


Fig. 2. Cross Section of Panel Thickness at Delamination Locations

## II. Theory

### Bifurcation Buckling

Bifurcation involves the transfer of membrane strain energy to bending strain energy. In a thin cylindrical panel, large deformation theory is required to indicate the relations depicting the membrane strain energy just prior to buckling in the form of bending strain energy. The best way to understand this phenomenon is to examine a typical load-displacement curve for a thin cylindrical panel loaded in compression (Fig. 3). Initially, the panel is loaded and the end-shortening of the panel follows the usual stress vs strain relations indicated by the early constant slope curve. At the bifurcation point, two paths are possible, one stable and one unstable. The upper straight extension of the linear end-shortening curve represents the unstable path. The lower curve or the stable equilibrium position is the buckled panel configuration. This is evident by the onset of large deformations mentioned previously.

### Classical Lamination Theory

To understand the behavior of composite laminates a basic understanding of the fundamentals of classical lamination theory is necessary. Only a

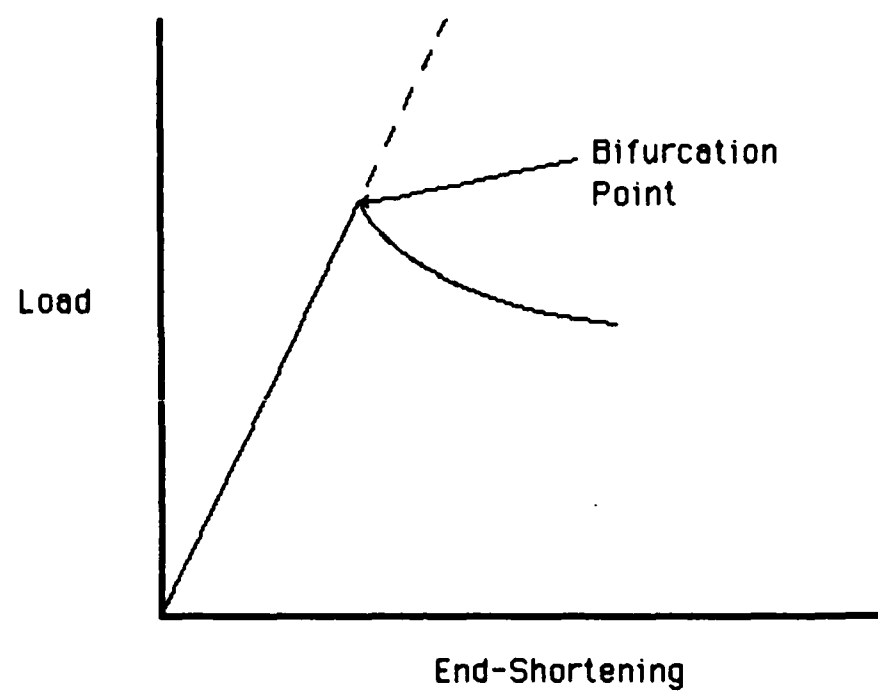


Fig. 3. Panel End-Shortening



brief explanation will be given here, but for the interested reader reference [11] provides a very detailed description of the theory.

Classical theory defines the strain-curvature relations for a laminate as follows:

$$\begin{Bmatrix} \epsilon_x \\ \epsilon_y \\ \gamma_{xy} \end{Bmatrix} = \begin{Bmatrix} \epsilon_x^0 \\ \epsilon_y^0 \\ \gamma_{xy}^0 \end{Bmatrix} + z \begin{Bmatrix} K_x \\ K_y \\ K_{xy} \end{Bmatrix} \quad (1)$$

where the superscript '0' indicates the mid-surface strains,  $z$  is the distance from the panel mid-surface, and the  $K$ 's are the mid-surface curvatures. These strains are multiplied by a reduced stiffness matrix to determine the corresponding stresses.

$$\begin{Bmatrix} \sigma_x \\ \sigma_y \\ \tau_{xy} \end{Bmatrix} = [\bar{Q}]_k \left[ \begin{Bmatrix} \epsilon_x^0 \\ \epsilon_y^0 \\ \gamma_{xy}^0 \end{Bmatrix} + z \begin{Bmatrix} K_x \\ K_y \\ K_{xy} \end{Bmatrix} \right] \quad (2)$$

The coefficients of the reduced stiffness matrix are functions of ply orientation in the layup and the material properties of the lamina. (The subscript  $k$  indicates one lamina).

Once the stresses in a layer are known, the resultant forces and

moments are obtained by integrating the stresses in each lamina through the total laminate thickness. The force,  $N_x$ , and moment,  $M_x$ , are expressed per unit length and are calculated by integrating the stresses over the laminate thickness as follows:

$$N_x = \int_{-t/2}^{t/2} \sigma_x dz \quad (3)$$

and

$$M_x = \int_{-t/2}^{t/2} \sigma_x z dz \quad (4)$$

The other forces and moments are similarly calculated. The positive direction of the forces and moments are shown in Fig. 4. Upon substituting Equation (2) into the above results, one obtains:

$$\begin{Bmatrix} N_x \\ N_y \\ N_{xy} \end{Bmatrix} = \sum_{k=1}^N [\bar{Q}]_k \left[ \int_{z_{k-1}}^{z_k} \begin{Bmatrix} \epsilon_x^o \\ \epsilon_y^o \\ \gamma_{xy}^o \end{Bmatrix} dz + \int_{z_{k-1}}^{z_k} \begin{Bmatrix} K_x \\ K_y \\ K_{xy} \end{Bmatrix} z dz \right] \quad (5)$$

and

$$\begin{Bmatrix} M_x \\ M_y \\ M_{xy} \end{Bmatrix} = \sum_{k=1}^N [\bar{Q}]_k \left[ \int_{z_{k-1}}^{z_k} \begin{Bmatrix} \epsilon_x^o \\ \epsilon_y^o \\ \gamma_{xy}^o \end{Bmatrix} z dz + \int_{z_{k-1}}^{z_k} \begin{Bmatrix} K_x \\ K_y \\ K_{xy} \end{Bmatrix} z^2 dz \right] \quad (6)$$

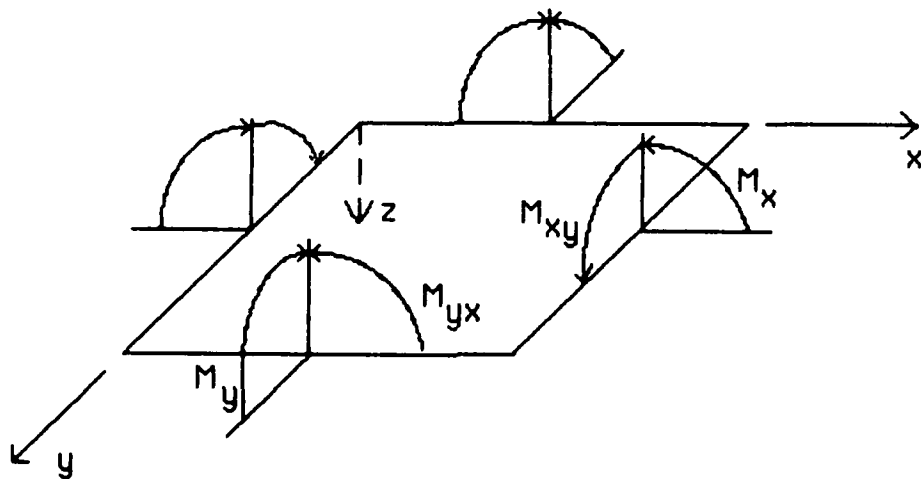
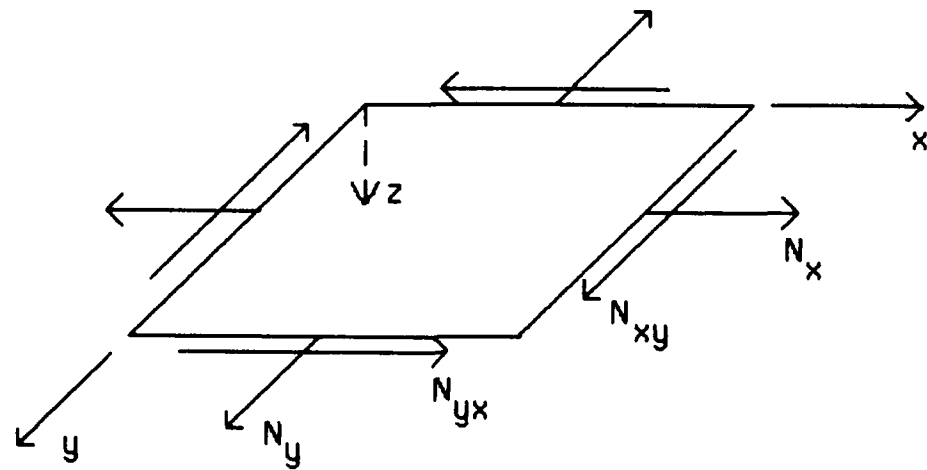


Fig. 4. Positive Directions of Forces and Moments

It is possible to simplify the above equation since the mid-surface strains are not functions of  $z$ . Therefore, they are removed from the integration and the force and moment equations become:

$$\begin{Bmatrix} N_x \\ N_y \\ N_{xy} \end{Bmatrix} = \begin{bmatrix} A_{11} & A_{12} & A_{16} \\ A_{12} & A_{22} & A_{26} \\ A_{16} & A_{26} & A_{66} \end{bmatrix} \begin{Bmatrix} \epsilon_x^0 \\ \epsilon_y^0 \\ \gamma_{xy}^0 \end{Bmatrix} + \begin{bmatrix} B_{11} & B_{12} & B_{16} \\ B_{12} & B_{22} & B_{26} \\ B_{16} & B_{26} & B_{66} \end{bmatrix} \begin{Bmatrix} K_x \\ K_y \\ K_{xy} \end{Bmatrix} \quad (7)$$

and

$$\begin{Bmatrix} M_x \\ M_y \\ M_{xy} \end{Bmatrix} = \begin{bmatrix} B_{11} & B_{12} & B_{16} \\ B_{12} & B_{22} & B_{26} \\ B_{16} & B_{26} & B_{66} \end{bmatrix} \begin{Bmatrix} \epsilon_x^0 \\ \epsilon_y^0 \\ \gamma_{xy}^0 \end{Bmatrix} + \begin{bmatrix} D_{11} & D_{12} & D_{16} \\ D_{12} & D_{22} & D_{26} \\ D_{16} & D_{26} & D_{66} \end{bmatrix} \begin{Bmatrix} K_x \\ K_y \\ K_{xy} \end{Bmatrix} \quad (8)$$

or

$$\begin{bmatrix} N_x \\ N_y \\ N_{xy} \\ M_x \\ M_y \\ M_{xy} \end{bmatrix} = \begin{bmatrix} [A] & [B] \\ [B] & [D] \end{bmatrix} \begin{Bmatrix} \epsilon_x^0 \\ \epsilon_y^0 \\ \gamma_{xy}^0 \\ K_x \\ K_y \\ K_{xy} \end{Bmatrix} \quad (9)$$

where  $A_{ij}$  are the extensional stiffnesses,  $B_{ij}$  are the coupling stiffnesses, and  $D_{ij}$  are the bending stiffnesses.

$$A_{ij} = \sum_{k=1}^N (\bar{Q}_{ij})_k (z_k - z_{k-1}) \quad (10)$$

$$B_{ij} = \frac{1}{2} \sum_{k=1}^N (\bar{Q}_{ij})_k (z_k^2 - z_{k-1}^2) \quad (11)$$

$$D_{ij} = \frac{1}{3} \sum_{k=1}^N (\bar{Q}_{ij})_k (z_k^3 - z_{k-1}^3) \quad (12)$$

Appendix A contains the  $A_{ij}$ ,  $B_{ij}$ , and  $D_{ij}$  matrices for the material properties of the graphite/epoxy used in this thesis for various thicknesses.

#### Delamination and Panel Buckling States

If one considers the buckling phenomena for composite panels with delaminations present, it is necessary to consider the state of instability of not only the overall panel but the individual delaminated thickness as well. Fei and Yin [8] defined three distinct states of buckling for a laminate with a delamination, namely, bifurcation, snap-through, and catastrophic failure.

They formulated a solution to the problem of a flat circular plate, loaded in compression, with a circular delamination located at its

geometric center. Pure in-plane compressive loading required to initiate buckling and growth of the delamination would be large in such a panel. However, if the laminate also undergoes bending deformation in addition to membrane compression, the thin delaminated layer will be subjected to a much higher compressive strain and may cause it to buckle and grow under a supercritical energy release rate. They indicated that the small deflections of the main body of the plate are governed by a global eigenvector equation. In the center of the plate, at the location of the delamination, the delaminated layer undergoes large deflections comparable to its thickness. Hence, von Karman's nonlinear theory of plates must be applied to obtain the governing equations. These equations are non-dimensionalized, and for any fixed ratio of the membrane strain to the bending strain in the plate, a one-parameter family of solutions of the non-dimensionalized problem is obtained by using an iterative procedure. With both bending deformation and membrane compression present, the delaminated layer maintains full contact with the main body of the plate until the deformation becomes sufficiently large and the delaminated layer experiences "snap-through." Snap-through is a condition where the delaminated layer buckles and no longer is in contact with the main body of the plate. The states of loading which will cause snap-through are determined by comparing the total strain

energy of the delaminated layer in the deformed states preceeding and following snap-through. Catastrophic growth of the delamination will occur when the energy release rate attains the critical value for growth.

The three non-dimensionalized expressions to describe the three states of buckling for the plate are a ratio of bending and membrane strain, delamination radius, and energy release rate. The three relationships are:

$$\rho = \mu h / 2\epsilon \quad (13)$$

where:

$\rho$  - bending strain versus membrane strain

$\mu$  - curvature to the plate middle surface

$h$  - depth of the delamination, measured from the top surface

$\epsilon$  - compressive membrane strain in delaminated layer

and

$$\tilde{a} = [12(1-\nu^2)\epsilon]^{1/2} a/h \quad (14)$$

where:

$\tilde{a}$  - non-dimensionalized delamination radius

$\nu$  - Poisson's Ratio

$\epsilon$  - compressive membrane strain in delaminated layer

$a$  - delamination radius

$h$  - depth of the delamination, measured from the top surface

and

$$\tilde{G} \tilde{a}^4 = [12(1-\nu^2)]^2 G^* a^4 / Eh^5 \quad (15)$$

where:

$\tilde{G}$  - non-dimensionalized energy-release rate

$\tilde{a}$  - non-dimensionalized delamination radius

$\nu$  - Poisson's Ratio

$G^*$  - material fracture toughness

$a$  - delamination radius

$E$  - Young's Modulus

$h$  - depth of the delamination, measured from the top surface

Fei and Yin present their results in tables and graphic form. The three non-dimensionalized values determine which buckling state the plate will experience. The value of  $\rho$  determines the value of  $\tilde{a}$  which will cause



snap-through. If  $\tilde{a}$  calculated in Eqn. (14) is larger than the value of  $\tilde{a}$  corresponding to  $\rho$  in Table 1 of Ref. [8] snap-through will occur. Finally, if  $\tilde{G} \tilde{a}^4$  calculated from Eqn. (15) is smaller than the corresponding  $\tilde{G} \tilde{a}^4$  contained in Table 1 of Ref. [8], then snap-through will be followed immediately by catastrophic growth. Based on the sample calculations in Appendix B, the eccentrically located total delaminations should snap-through. However, no delamination growth should occur.

#### STAGSC-1 Theory

STAGSC-1 (Structural Analysis of General Shells) is a finite element computer code based on the variational method. The April 1983 version of the code is used in this thesis. The purpose of this code is to analyze shell structures constructed with non-isotropic materials with various loadings and boundary conditions. There are 20 different elements which can be used with this code. The finite element used in this thesis is the 410 element since it was found to produce virtually the same results ( $\pm 2.0\%$ ) as the 411 element, but is more cost effective to run. The 410 element has 24 degrees of freedom and is not compatible with curved surfaces in some cases. For the problem being analyzed here, this does not affect the results significantly if a sufficient number of elements are used. The panel was divided

into 2/3 inch square elements for the analysis. References [12,13,14] give further information on the theory behind STAGSC-1.

The material properties used in STAGSC-1 were determined experimentally for a given ply of AS4/3501-6 graphite/epoxy to be:

$$E_1 = 18.844 \times 10^6 \text{ psi}$$

$$E_2 = 1.468 \times 10^6 \text{ psi}$$

$$G_{12} = 0.910 \times 10^6 \text{ psi}$$

$$\nu_{12} = 0.280$$

$$G^* = 0.7423 \text{ in-lbs/in}^2 \quad [19]$$

The boundary conditions incorporated into the STAGSC-1 analysis are the same as those assumed in the experimental test device (a clamped top edge ( $u = v = w = w_{,x} = 0$ ), clamped bottom edge ( $u = \text{free}, v = w = w_{,x} = 0$ ), and simply supported vertical sides ( $u = v = w_{,y} = \text{free}, w = w_{,x} = 0$ )). Fig. 1 shows the panel axis system.

#### Experimental Techniques to Evaluate Defect Size and Location in Composites

The problems associated with examining composite structures with

delaminations or damage of any kind are numerous. For structures where the only damage is located between the same two plies in the entire laminate, traditional x-ray or C-scan techniques will suffice. However, for through the thickness damage, determining the nature and location of the delaminations or damage is impossible with a one-dimensional technique. Therefore, three-dimensional examination techniques are needed for this problem. There are two methods which are used namely, stereo x-ray and depty tech- niques.

Stereo radiography is a simple procedure where two x-rays of the same object are taken from two different orientations [15,16,17]. The x-ray set-up is shown in Fig. 5. The maximum angle,  $\beta$ , is determined by the material properties and dimensions of the specimen. The two different orientations are obtained by rotating the specimen 180 degrees on the platform between x-rays.

In this procedure, a hole is drilled in the specimen through the damaged region and a penetrant, tetrabromoethane (TBE), is applied to the specimen through the hole. The penetrant is applied continuously for 30 minutes to allow adequate time to saturate the damaged region. The TBE causes a contrast between the damaged and the undamaged areas in the x-rays. After 30 minutes, the x-rays are taken.

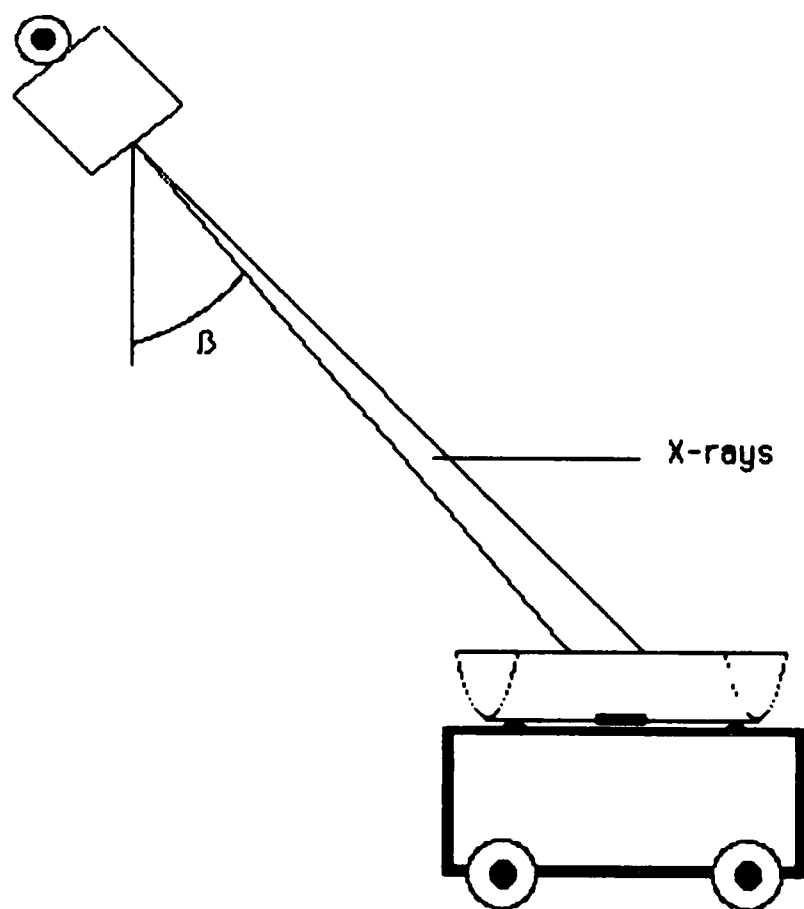


Fig. 5. Stereo X-ray Arrangement

The two x-rays must be merged together to visualize the three dimensionality of the damaged region. There are several methods to accomplish this; the easiest being with a stereoscope. If a stereoscope is used, then photographic prints from the x-rays are required. The pictures or stereo pair are viewed through the stereoscope and the eyes merge the pair together into a three dimensional picture. A more detailed explanation of this process is found in references [17,18].

The deplying technique is a newly developed destructive technique for examining composite laminates. With this technique, the specimen to be deplyed has a hole drilled through the damaged region. A gold chloride solution is applied through this hole into the damaged laminate and allowed to penetrate for approximately 30 minutes. After the gold chloride solution has saturated the area, the excess is wiped from the surface and the sample is heated to approximately 150<sup>0</sup> F to remove the solvent before proceeding with the deplying. The specimen is placed on a wire mesh holder and placed in a furnace. The furnace's temperature is maintained between 785<sup>0</sup> F to 800<sup>0</sup> F for 70 - 100 minutes. The partially pyrolyzed (chemically broken down using heat) sample is removed from the furnace and allowed to cool to room temperature. The laminate is unstacked by placing adhesive tape on the top ply and lifting it off. This process is continued through the

thickness and the individual plies are examined visually or with the aid of a 0-80 X scanning microscope. The damaged or delaminated areas are highlighted with a light colored gold residue [14].

### III. Manufacturing and Experimental Procedures

#### Panel Manufacturing

The panels used in this research activity are fabricated from Hercules AS4/3501-6 graphite/epoxy 12 inch prepreg tape. The layup for all the panels fabricated is  $(0/-45/+45/90)_5$ . As mentioned earlier, partial delaminations are typical of low velocity projectile impact damage. Therefore, in order to simulate this impact phenomenon, panels were manufactured with pre-existing partial delaminations. Based on previous work [1], mylar was chosen as the partial delamination causing insert.

Initially, a flat test panel was fabricated using five 1 mil mylar inserts with a coating of Ram 225 release, one between each of the inner plies as shown earlier, to determine if the panels could be made. The five inserts in this trial panel caused the matrix in the outside  $0^0$  fiber orientation plies to fracture during the curing cycle. In addition, the 1 mil mylar inserts added an equivalent extra ply to the panel. Thus, to overcome some of these shortcomings, 0.5 mil mylar inserts were chosen in the fabrication of another test panel. The five 0.5 mil mylar inserts did not cause any curing fracture in the exterior plies and a C-Scan of the fabricated test panel indicated that the inserts did cause a partial delamination, as expected.

The C-scan also showed that the inserts did not move during the curing process, therefore, mylar was chosen for the delamination causing insert material.

The curved panels were laid up in sets of four, in large curved molds (Fig. 6) with the required 12 inch radius of curvature. A mylar template was used to accurately place the mylar inserts in the proper locations (Fig. 7). A planning sheet was also used to ensure that the inserts were both placed between the correct number of plies and the correct plies. After the panels had been laid up, they were prepared for the autoclave and sealed in a nylon bag (Fig. 8). Four of the large molds were placed in the autoclave (Fig. 9) and cured using the following cure cycle:

- (1) Apply full vacuum (25 in. Hg. minimum) and 85 psi
- (2) Heat air to  $240^{\circ}\text{F} \pm 5^{\circ}$  in 30 minutes
- (3) Hold part at  $240^{\circ}\text{F} \pm 5^{\circ}$  and full vacuum for 60 minutes under 85 psi
- (4) Increase the pressure in the autoclave to 100 psi and then vent vacuum
- (5) Heat air to  $350^{\circ}\text{F}$  in 30 minutes  $\pm 5$  minutes
- (6) Hold part at  $350^{\circ}\text{F} \pm 5^{\circ}$  and 100 psi for 120 minutes
- (7) Cool part below  $150^{\circ}\text{F}$  in less than 120 minutes
- (8) When below  $150^{\circ}\text{F}$ , vent pressure





Fig. 6. Layup of Four Small Panels In One Large Mold



Fig. 7. Mylar Template Used To Place Delamination Causing Insert

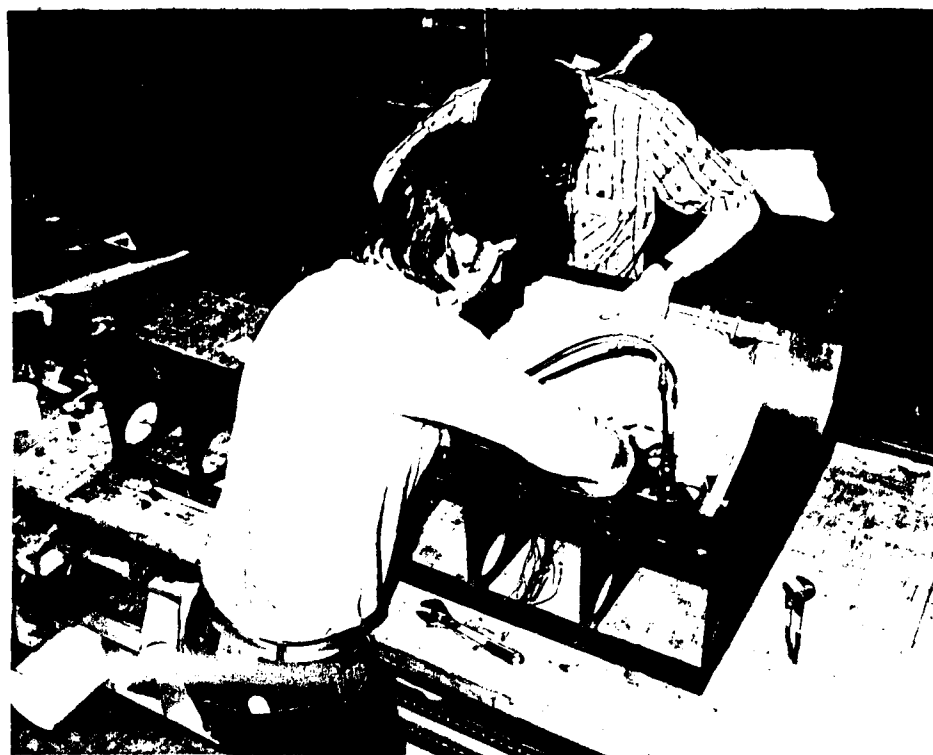


Fig. 8. Large Panel Sealed In Nylon Bag

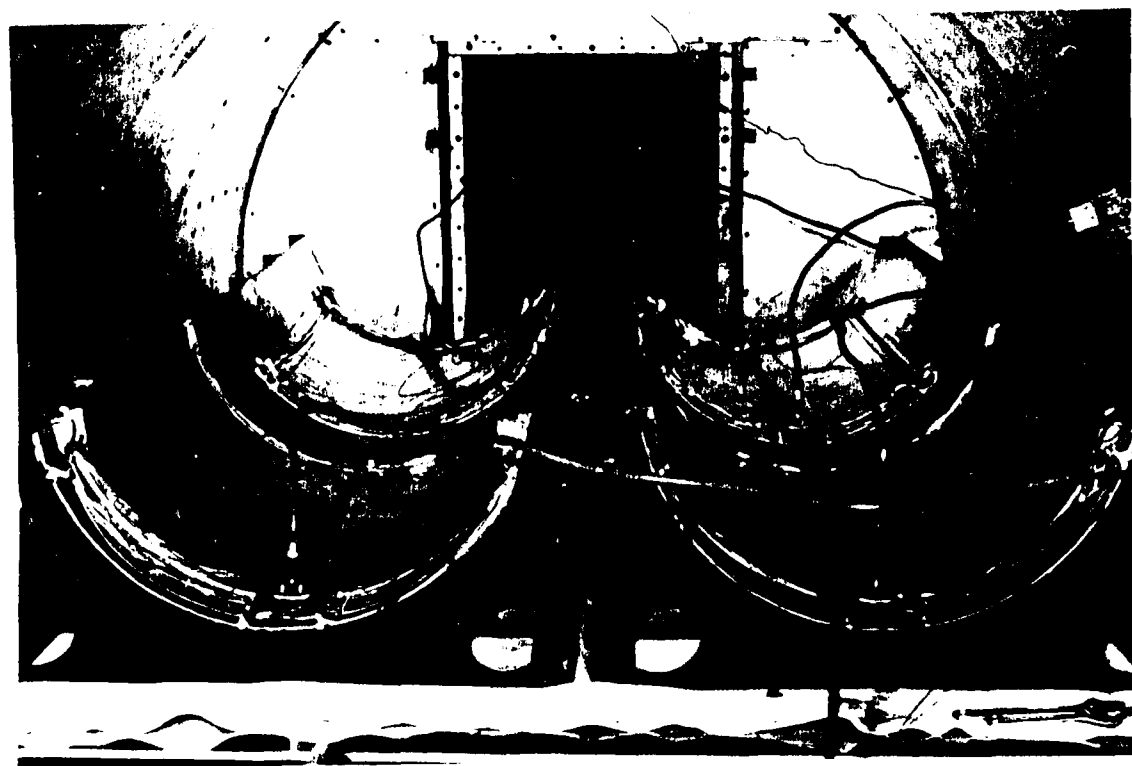


Fig. 9. Four Large Panels In Autoclave

Upon completion of the curing cycle, the large panels were C-scanned to determine if there were any voids present, if the delaminations were present and to insure that no movement had occurred during the curing process. The C-scan results showed that the partial delaminations were present and had not moved. Therefore, the original mylar template method used in the lay-up process was also used in marking the partial delamination locations.

A final set of test panels were fabricated using 2 mil teflon inserts with Ram 225 release. Teflon was chosen because it does not bond well with graphite/epoxy, and it has been incorporated in previous studies [2] with success. The same lay-up process and cure cycle were applied to these panels. The subsequent C-Scan results showed the presence of a good dis-bond in the laminate with the teflon inserts. The validity of the C-scan results will be discussed in the Results and Discussion section. These panels are used as the baseline for the effect of delaminations in graphite/epoxy curved panels.

Four smaller panels were then cut from each of the larger panels to the approximate size of 13 inches in length and 12 1/2 inches in chord. All cutting was done with a radial arm saw using a diamond tipped blade. Fifteen thickness measurements were taken and averaged for each of the small panels to obtain an average panel thickness. Previous experiments

[1,3,4] indicate that uniformity of the length dimension is critical for uniform load introduction. Therefore, a special tool was built to secure the panels as the final length dimensions were being cut. Length dimensions, which varied less than 10 mils, were found to be acceptable [1,3,4]. The fixture shown in Fig. 10 was used to cut the length dimension of the panels. It produced results with no variation greater than 3 mils. The dimensions of the vertical sides were less important as a 1/4 inch gap was available at the vertical side supports to eliminate any impact from a size difference in the chord of the panels.

#### Experimental Set-Up

A 30K lb capacity compression test machine was incorporated in this study to generate the buckling loads for the test panels. This device used special fixtures to hold the curved panels. These fixtures were assumed to give the following boundary conditions; clamped top edge ( $u = v = w = w_{,x} = 0$ ), clamped bottom edge ( $u = \text{free}, v = w = w_{,x} = 0$ ), and simply supported along both vertical sides ( $u = v = w_{,y} = \text{free}, w = 0$ ).

The clamped top and bottom boundary conditions are obtained by using the steel plates shown in Fig. 11. The panel is placed in the top and bottom



Fig. 10. Length Dimension Being Cut Using Special Fixture

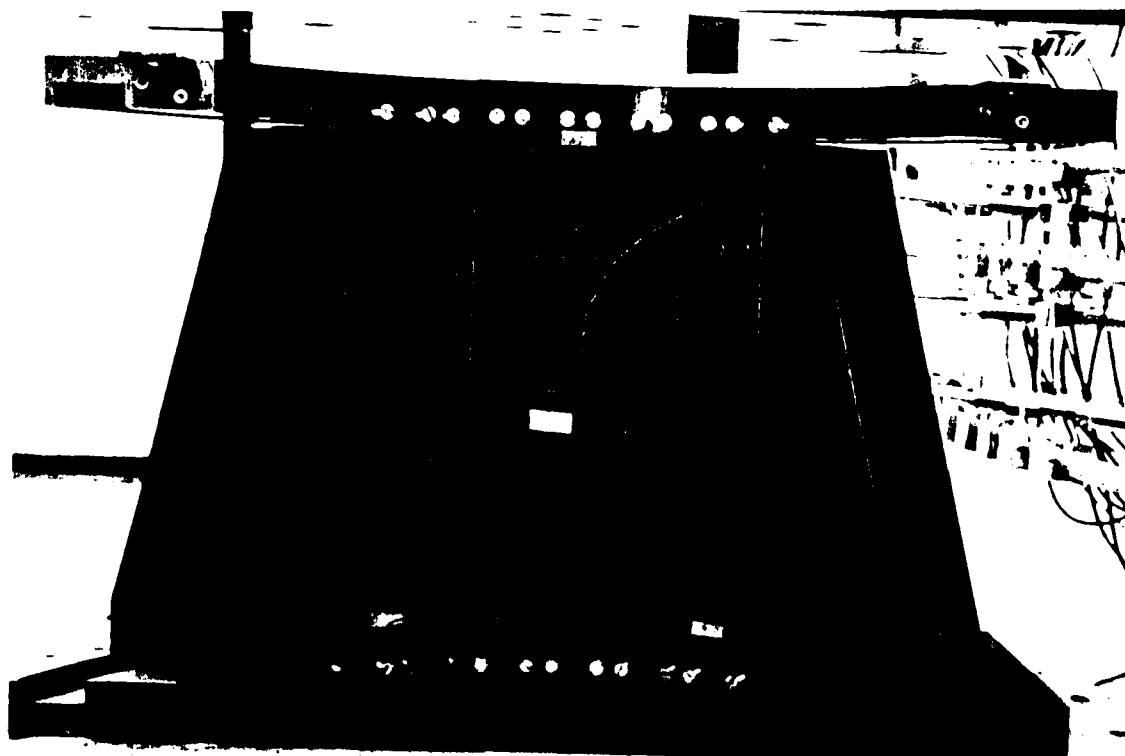


Fig. 11. Steel Plates for Top and Bottom Boundary Conditions

slots and centered. Small steel wedges are butted against the panel and are held in place by screws which are tightened with a screwdriver. The wedges are shown near the bottom of the panel in Fig. 12. The top and bottom plates are centered with a removable bolt which goes through the plates and into the respective top and bottom surface of the test fixture. This exact centering is done for each test panel and ensures consistency and removes any load eccentricities.

The simply supported boundary conditions along the vertical sides are developed by using knife edges. Previous work [1,2] has shown this boundary

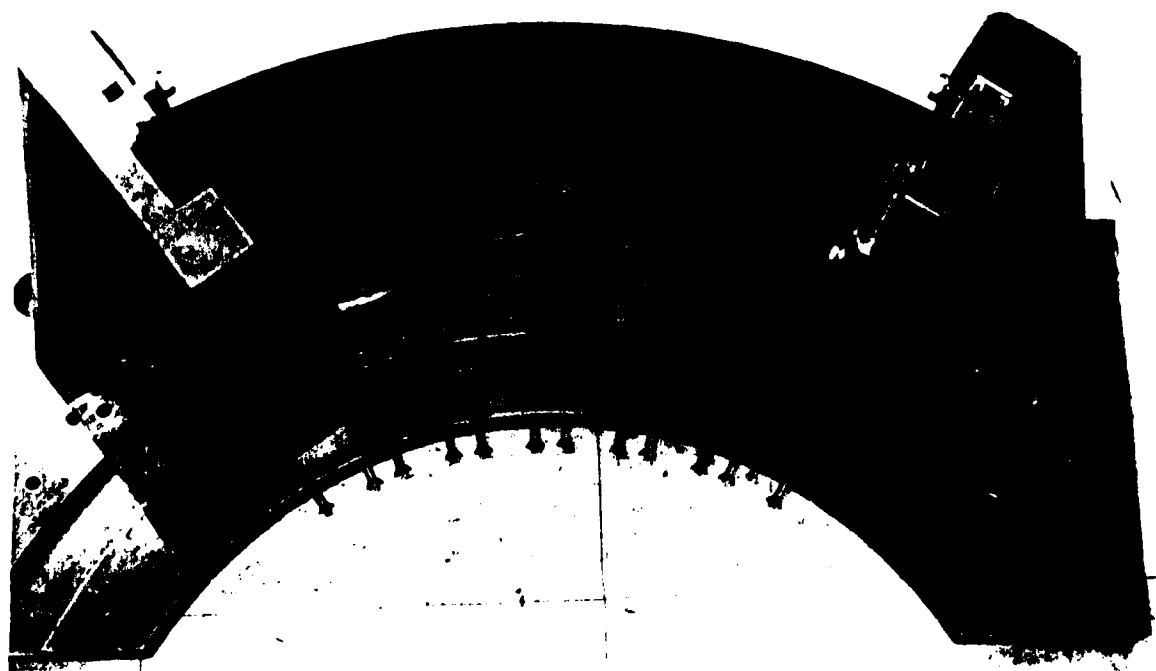


Fig. 12. Panel In Test Fixture Showing Steel Wedges

condition is difficult to obtain. To better obtain this condition, the test fixture was modified with the addition of an "O" ring to the knife edges to keep a constant pressure against the test panel (Figs. 13, 14). Also, to aid u and v movement, a strip of teflon tape was applied to both sides of the vertical edges of the panels before installation in the fixture. The teflon tape is shown (Fig. 14) near the top of the panel where it has been loosened.

The same installation procedure was followed for each of the test panels. The panel was placed in the test fixture frame ensuring that it was centered. The top and bottom edges were clamped first, followed by the installation of the vertical side supports. A 1/4 inch gap between the vertical side supports and end supports allows for compression of the panel. This gap was placed at the bottom because more consistent results were obtained in the past [1,2]. The testing of several panels showed that placing the knife edges in the center of the panel with 1/8 inch at the top and bottom supports yielded more consistent buckling loads and symmetric buckling patterns. The complete experimental set-up is seen in Fig. 15 with the exception of the front LVDT (Linear Variable Differential Transformers). The compressive load is introduced through the bottom with a hydraulic ram. This forces the bottom test bed frame up, guided by the vertical sleeves of

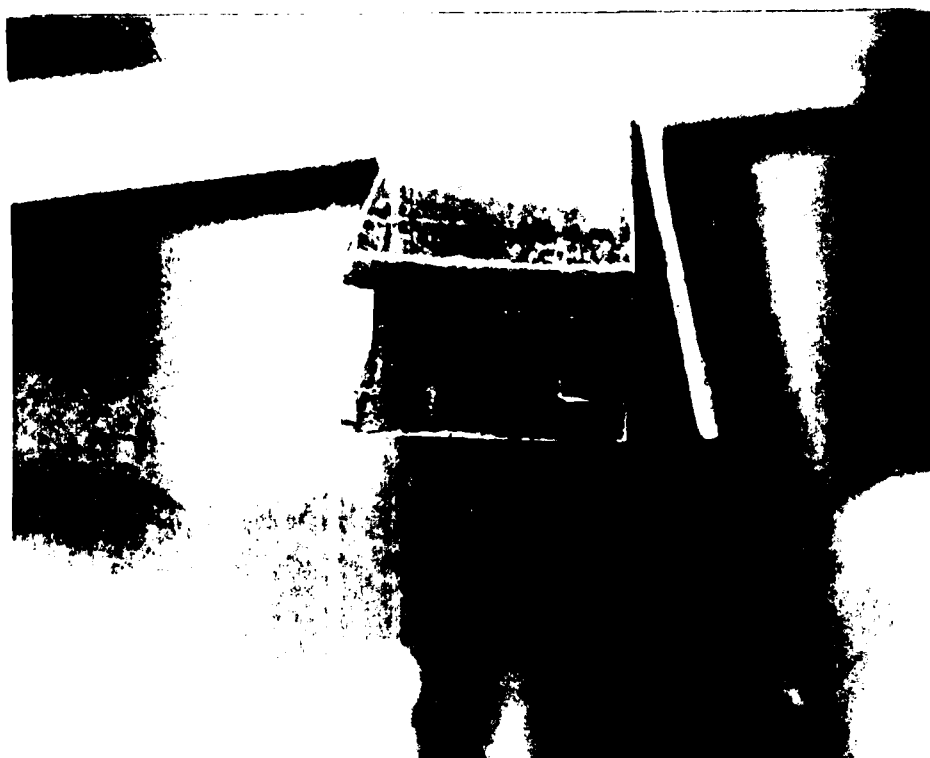


Fig. 13. Knife Edge with "O" Ring

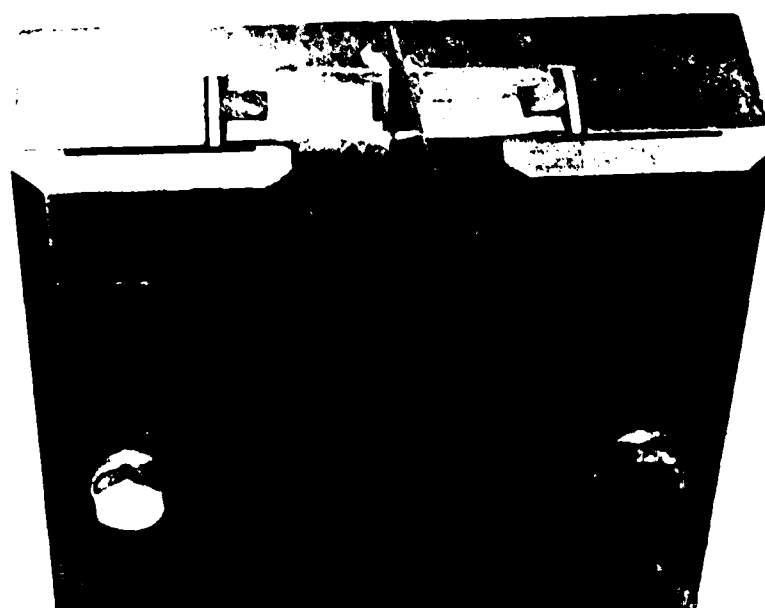


Fig. 14. Knife Edge Installed In Vertical Support



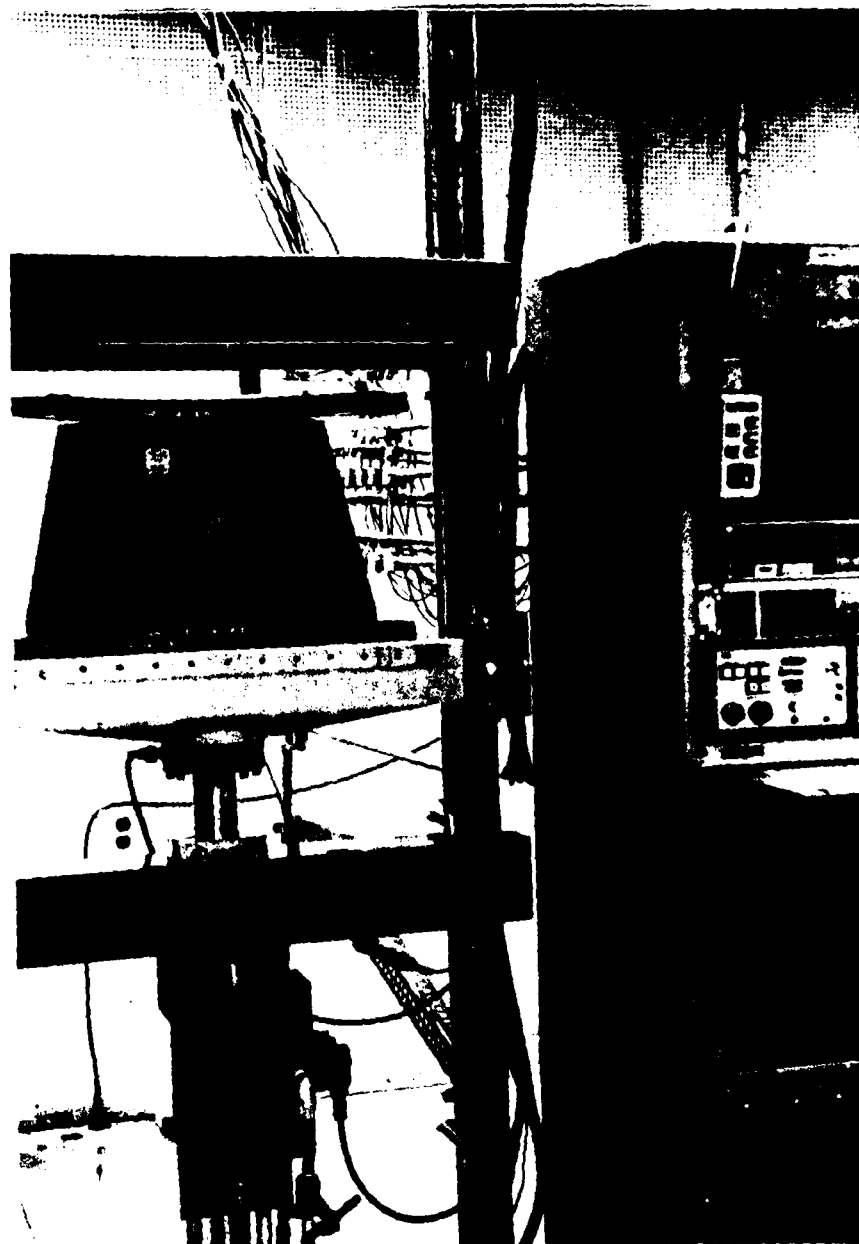


Fig. 15. Complete Experimental Setup

the machine.

The instrumentation used to collect data includes four axial strain gages and 16 LVDT displacement transducers. Two strain gages are positioned back to back at the geometric center of the delamination and the panel. These are used to measure the local strain which in turn is associated with both the local buckling of the delaminated area and the global buckling of the panel. The remaining two gages are placed one inch from the bottom and two inches from either outer edge of the panel. The strain data gathered from these gages are used to check for even load introduction. One LVDT, mounted in front of the inside surface of the panel between the top and bottom supports, is used to determine the global buckling load by measuring end shortening. The remaining 15 LVDTs are spaced equi-distant in three rows on the outer surface of the panel (Fig. 16). The data obtained from this matrix of displacement measurements produce an overall picture of the panel's radial movement as it is loaded. They are also used to show a rough approximation of the buckled shape of the panel.

### Test Procedure

Once the panel is installed, the four strain gages are electronically zeroed. The front LVDT is calibrated prior to testing and the accuracy of

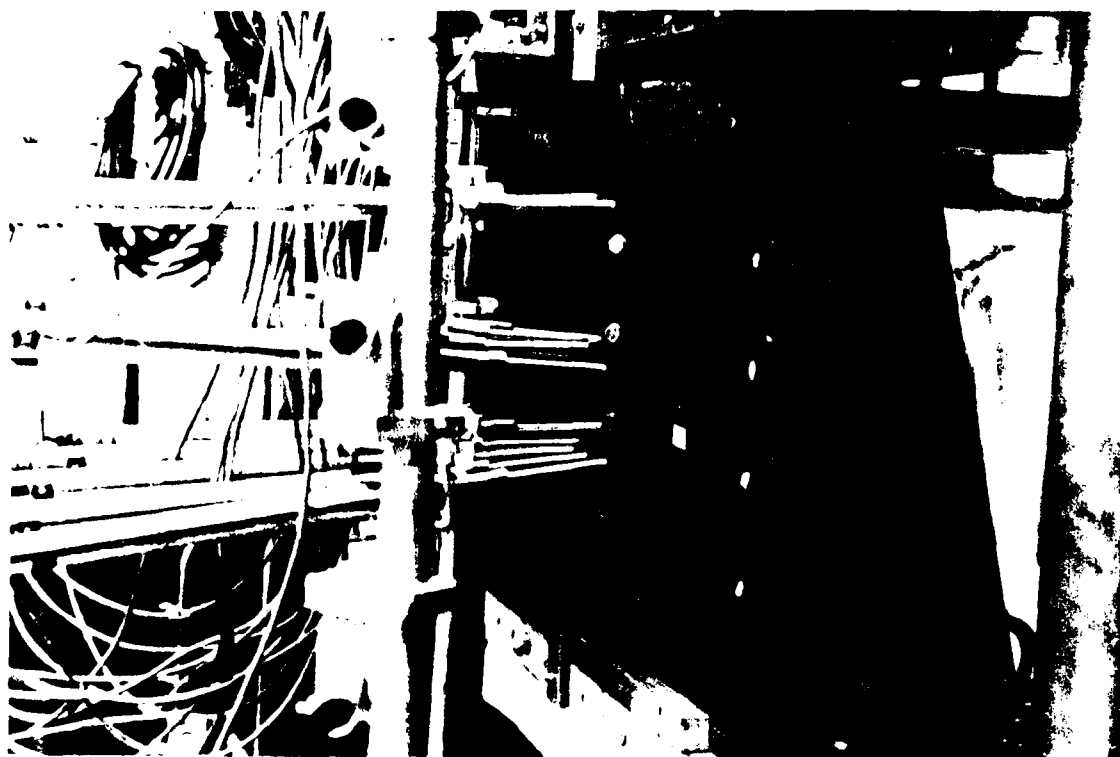


Fig. 16. Outer Surface LVDTs

any measurements taken are valid only in this range. The LVDT is adjusted in its fixture to ensure it will be operating in its calibrated range. As a result of their holding fixture, the remaining 15 LVDT's are automatically within their calibrated range and no adjustment is necessary. The compressive load is then introduced at a constant 0.05 inches per minute. The data were taken four times every second and stored in real time on a VAX 11/780 computer. The data were printed out and plotted. The load rate was kept constant until the panel buckled globally and then the machine was placed on hold. This allowed the buckling pattern to be highlighted with a silver pencil and photographed. The load and strains could be monitored on a CRT during the test and any interesting phenomenon both from the CRT and visually were noted.

#### IV. RESULTS AND DISCUSSION

##### Panel Identification

To allow for easy handling and identification of the different experimental panels, the panel identification scheme shown in Table I is used.

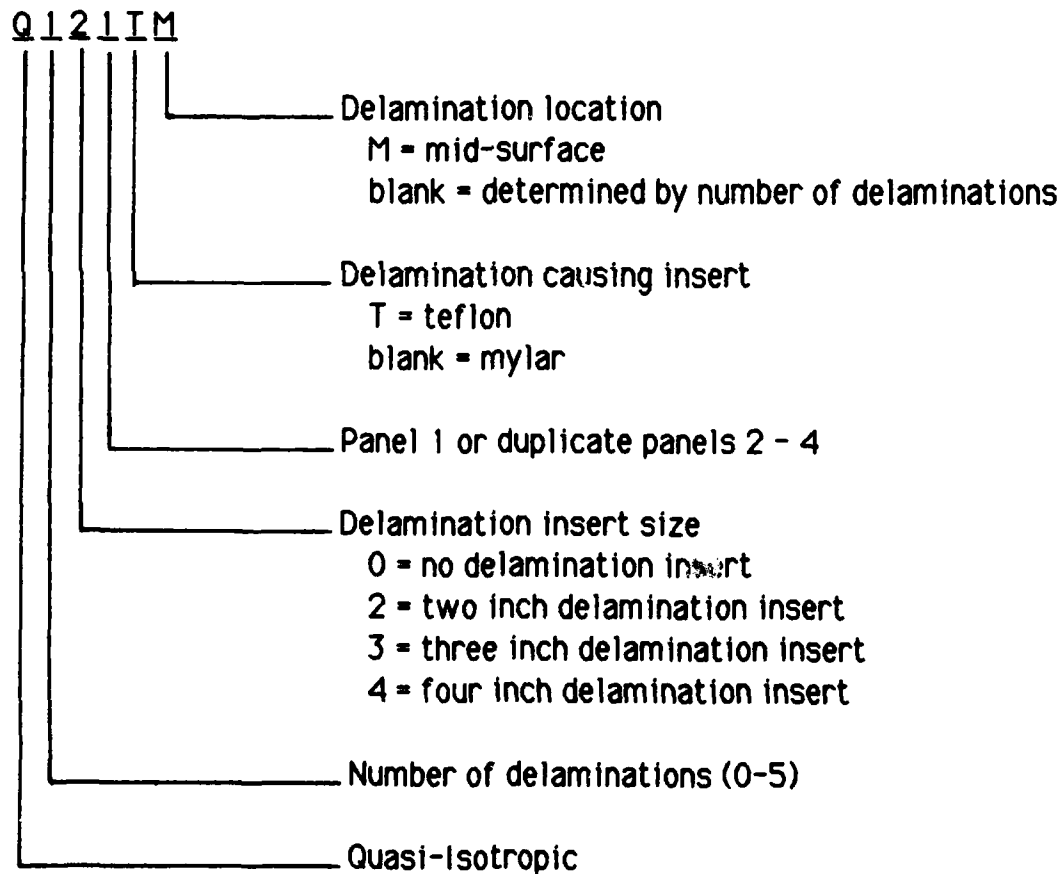


Table I. Code Representation for Panels Incorporated In This Study

A code with duplicate panel number missing will indicate an average for all panels of that particular delamination size and type. For example, Q12TM defines an average of the values for panels Q121TM, Q122TM, Q123TM, and Q124TM which has one teflon insert located at the laminate mid-surface (Fig. 2).

Figures 17 and 18 show the delamination locations for panels Q12 and Q22 respectively. Panel Q32 would simply have one additional delamination added to the layup of Q22 between plies four and five. A similar process is carried out for Q42 and Q52 panels.

#### Data Output

The data obtained from each panel are assigned a run number which correlate to the number given to the hand written observations for each panel taken during the testing. These handwritten observations may include; any snapping during loading, the buckling pattern, local buckling at the delamination, and any peculiarities observed during the test. The rest of the data are printed and plotted later. The printed data are all referenced to an internal computer time which allowed any channel to be compared to any other during the test for a given panel. In addition to the printed data, six computer plots were generated for each buckling test. Two plots, load

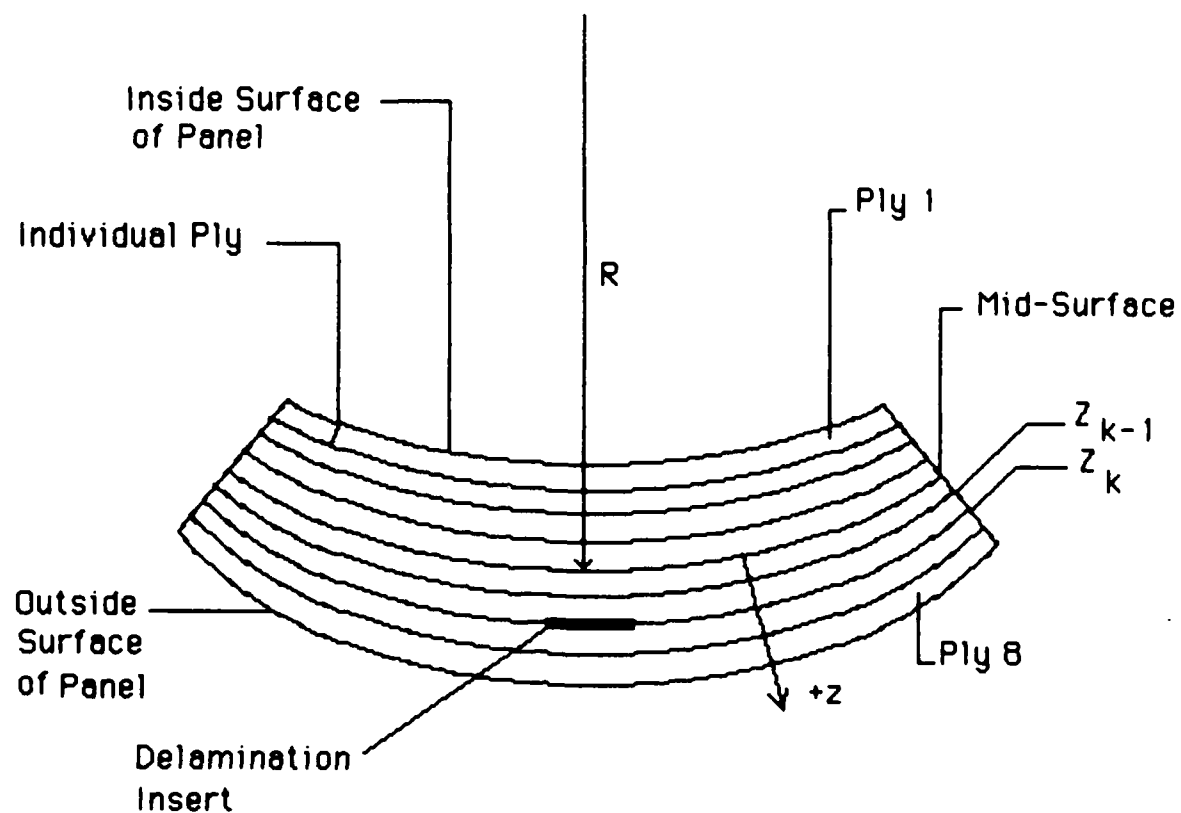


Fig. 17. Cross Section of Panel Q12 at Delamination Locations

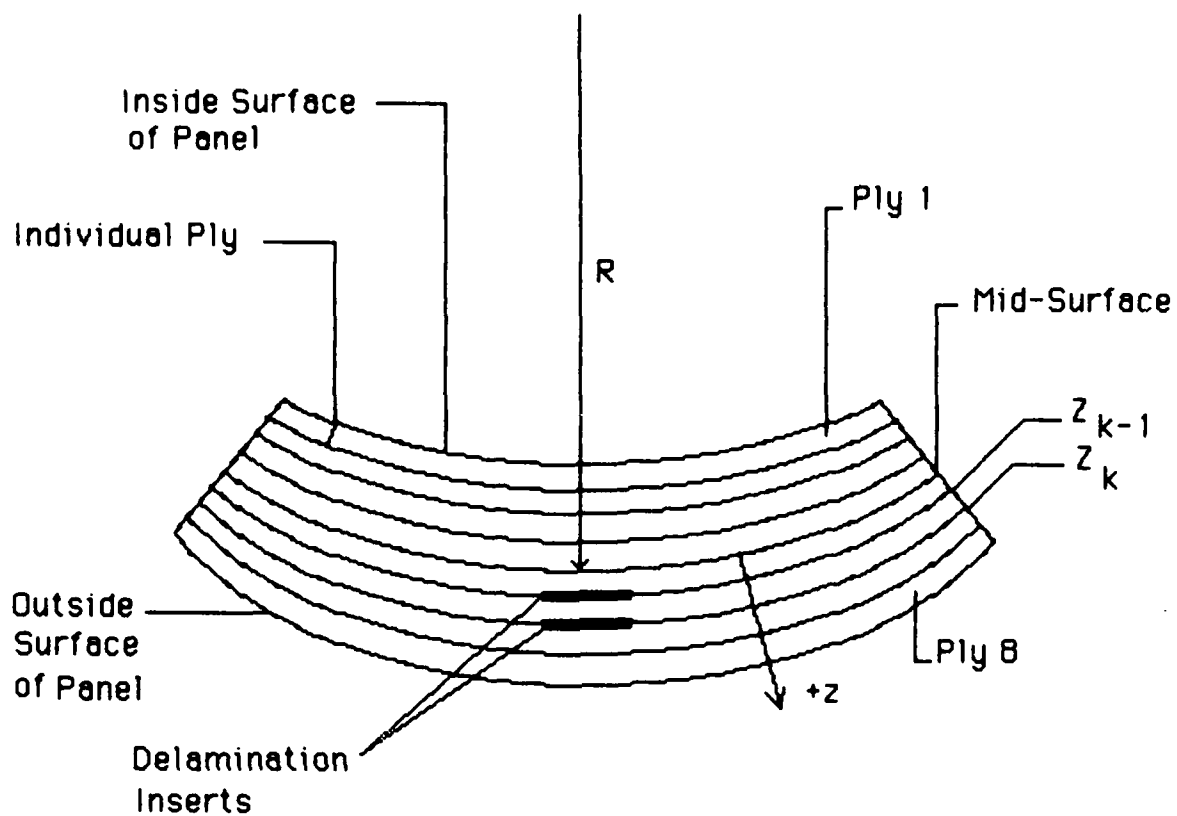


Fig. 18. Cross Section of Panel Q22 at Delamination Locations



versus panel end-shortening and load versus back-to-back strain gages, are used to determine the buckling load for the panel. A third plot included load versus the two remaining gages as a check for even load introduction. The remaining three plots contain the data from the outer surface LVDT's arranged in three rows of five to display the load versus radial deflection of the panel for a given row of LVDT's.

The two techniques to determine the buckling loads, load versus end-shortening (Fig. 19) and strain reversal (Fig. 20), yielded identical results. This is due primarily to the catastrophic nature of the panel buckle. With the end-shortening method the panel shortens linearly until the panel becomes unstable and collapses. With the strain reversal technique, the back-to-back strain gages both show a compressive load until the panel again becomes unstable and buckles. This causes the strain gages to immediately read differently as the result of the sudden introduction of bending strains. Figures 21 and 22 are actual test data plots for panel Q123T, one delamination caused by a teflon insert (Ref. Table I), used to determine its buckling load. Figure 22 shows that, although the back to back gages do not show a linear compression on both faces as the load increases, the nature of the buckle causes a severe drop in the strain gage readings. The divergence of the two strain readings is attributed to the snap-through phenomenon

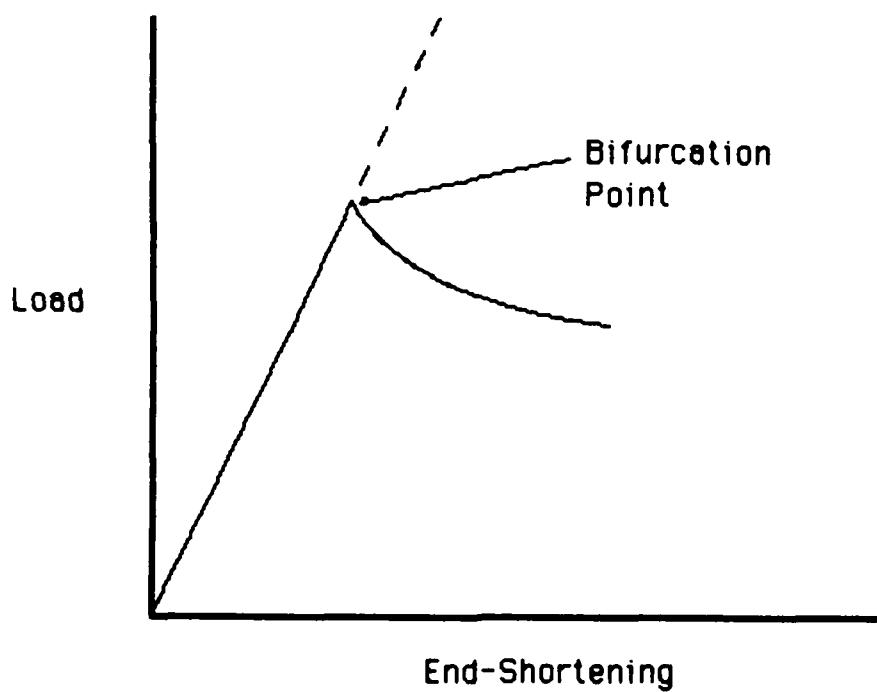


Fig. 19. Panel End-Shortening

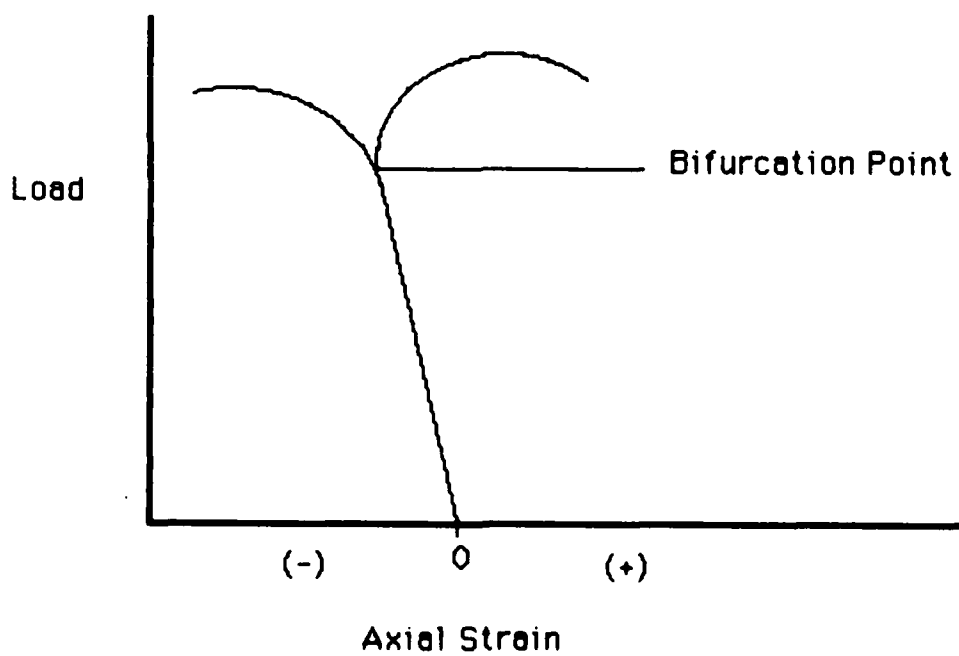


Fig. 20. Strain Reversal

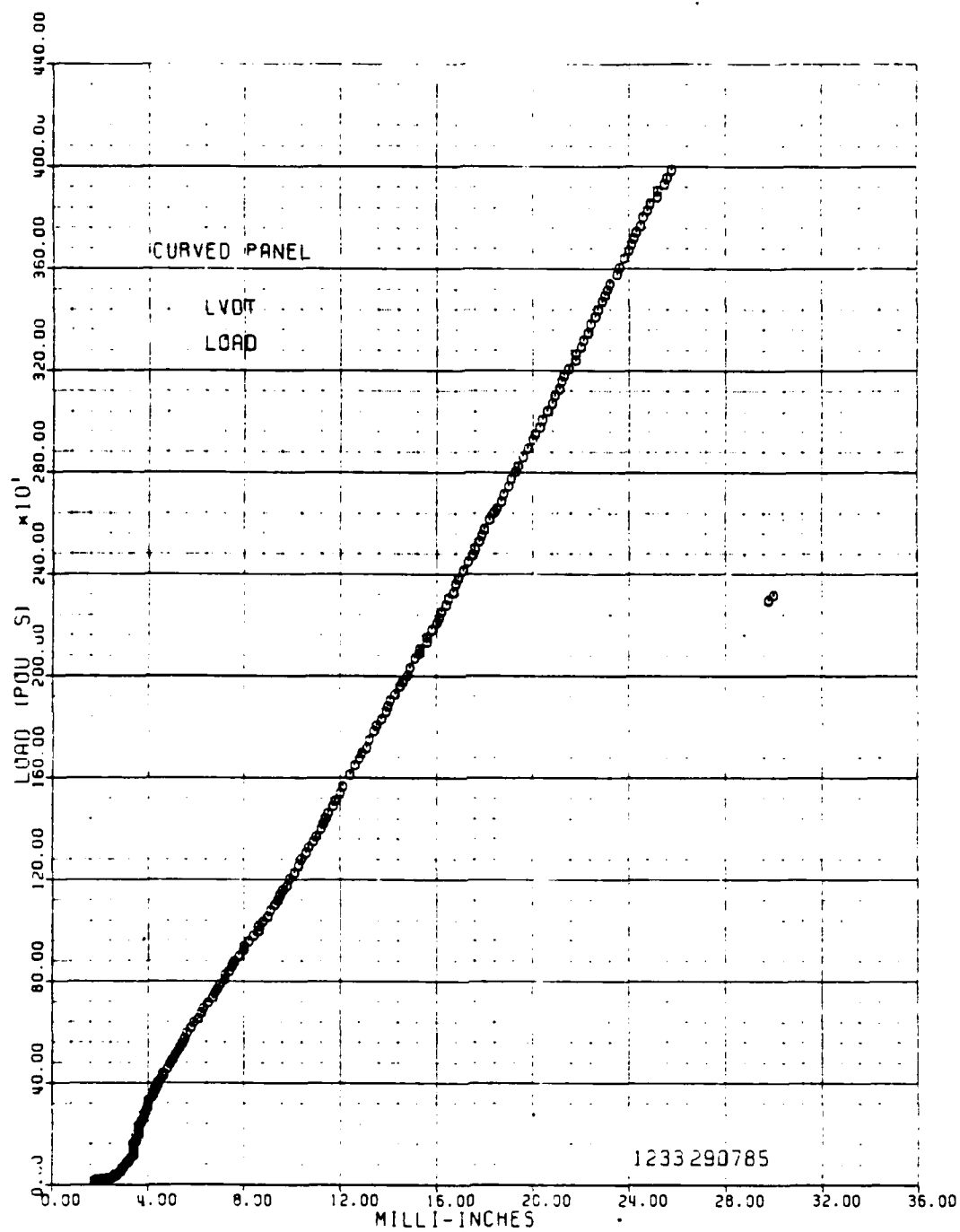


Fig. 21. Panel Q123T End-Shortening

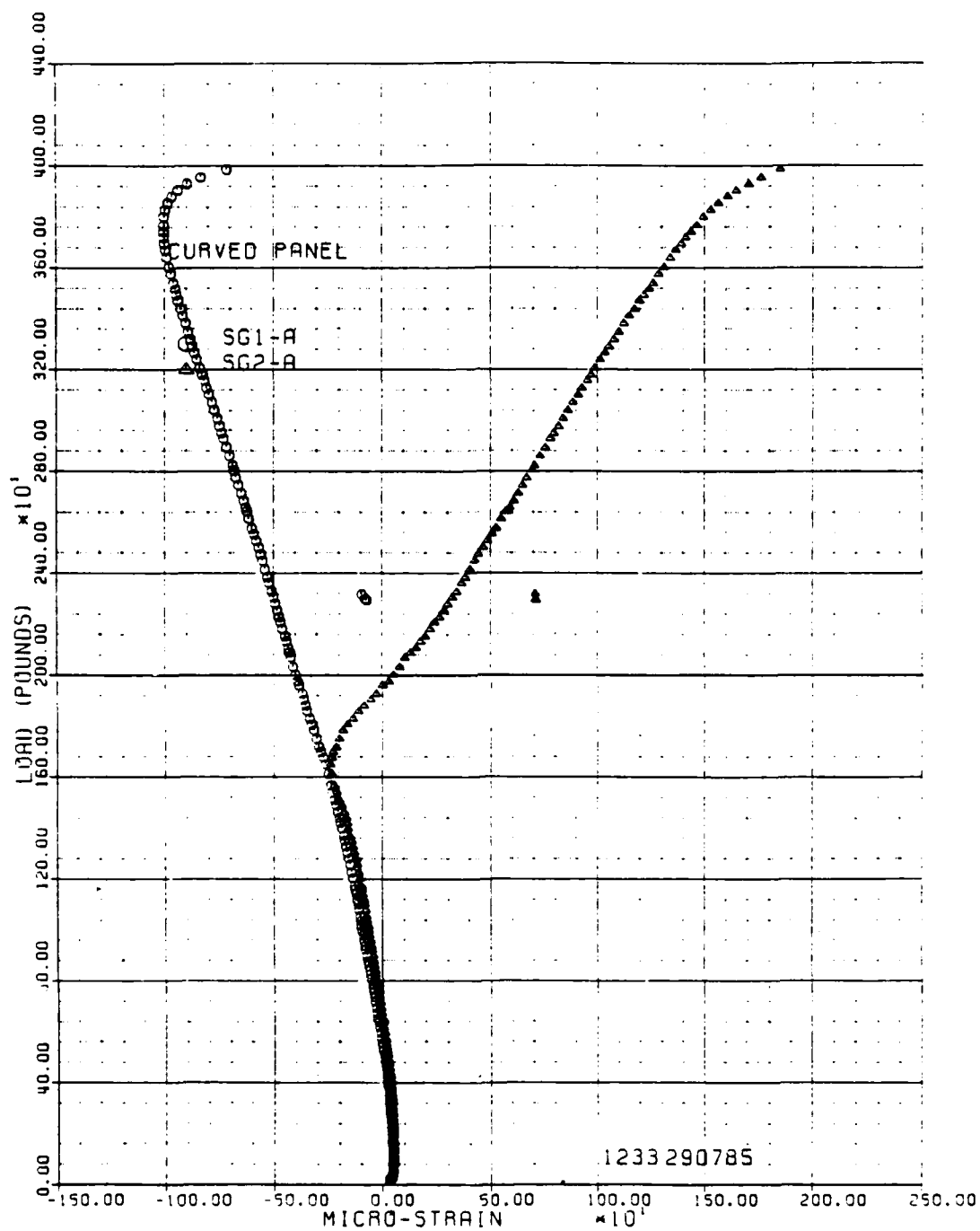


Fig. 22. Panel Q123i Strain Reversal

predicted by Fei and Yin [8]. The snap-through effect will be discussed in more detail in the Buckling Pattern section.

Appendix C contains the experimental results for the test panels. Data for all panels are not included since the data from some panels were judged unreliable. Panels were eliminated based on the buckling shape, unusual phenomena noted during the test, and obvious large uneven load introduction. The panels with the mylar inserts have not been corrected for the amount of actual delaminated area. For instance, a panel with five inserts may have less delaminated area than a panel with three inserts, and this has not been accounted for in the data in Appendix C.

#### Analytical/Experimental Comparison

Since there are no analytical models or computer codes which are designed to predict the behavior of laminates with delaminations, the experimental data obtained herein are compared to the STAGSC-1 results. The test data are normalized to the STAGSC-1 buckling load for a panel of equal thickness with no delaminations. These normalized results are shown in Appendix C and expressed as percent knockdown from the STAGSC-1 buckling load.

The test fixture provides the boundary conditions for which it was

designed. The panels with no delaminations present, Q00, only had a knockdown factor of 8.3 %. A knockdown factor this low for a buckling test indicates very good results, especially when considering all the variables which effect a compression test. From observing the testing, it is clear that the only boundary condition which may not have been correct is free movement in the y direction. This was evident from scarring on the teflon tape on the vertical sides in the y direction. The STAGSC-1 modeling with  $v = \text{fixed}$  on the vertical sides showed 13 % higher buckling loads than STAGSC-1 results with  $v = \text{free}$ . The experimental results were lower than both of these results which means that the knockdown factor was probably somewhere between 8.3 % and 21.3 %. Even with this 21 % value the results are favorable. For comparison purposes, it was decided to make comparisons with STAGSC-1 using the free circumferential boundary ( $v = 0$ ) along the vertical edges.

The results of the panels with teflon inserts or total delaminations present revealed, as expected, an increasing knockdown factor with increasing delamination size. Fig. 23 shows this effect with a plot of knockdown factor versus delamination area for panels Q00, Q12T, Q13T, and Q14T. The end-shortening of the panels with total delaminations also produce expected results. It can be observed in Fig. 24 that the panels with the larger

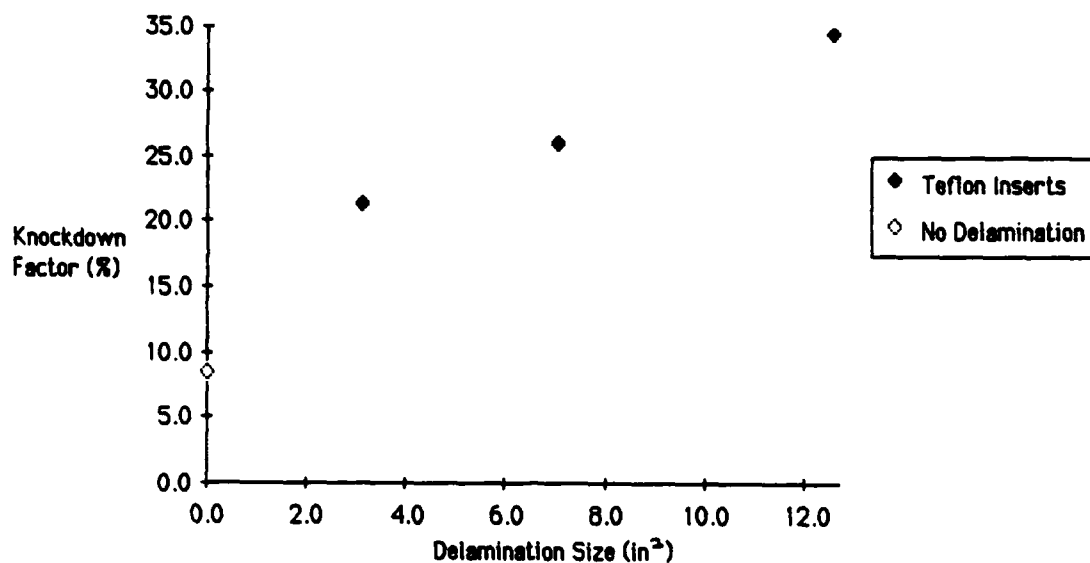


Fig. 23. Knockdown Factor vs Delaminated Area at Buckling  
(Panels With Teflon Inserts)

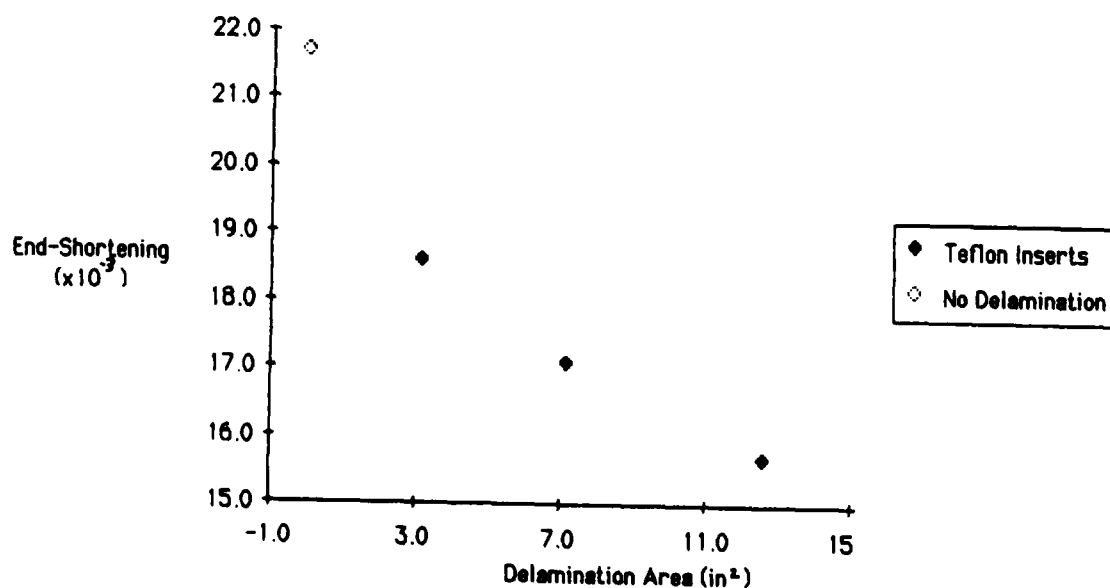


Fig. 24. End-Shortening vs Delaminated Area at Buckling  
(Panels With Teflon Inserts)

delaminations do not deform as much before buckling as the panels with less delaminated area present. This is a good indication that these particular panels have less strain energy present before buckling.

### Buckling Patterns

To understand the buckling shape of the panels an understanding of the panel movement prior to buckling is helpful. During loading, the panel displaced away from the center of curvature. This movement is shown in figures 25 and 26. These figures show the movement of the vertical and horizontal planes of symmetry, respectively. The area where the delamination is located moved in the opposite direction (Fig. 25 and 26), toward the center of curvature, as the rest of the panel just prior to buckling. This movement is detected with the center row of LVDTs. This movement is the snap-through effect that Fei and Yin predicted [8].

The snap-through effect is not as obvious as it might have been with a flat plate. This is due to the circumferential stress developed due to the deflection of the panel as the load is increased. The strain in the y direction was measured on Q123T, Q134T, and Q144T (Ref. Table I) with a strain gage rosette (1/8 inch) in place of the normal axial gages in the center of the delamination. These measurements indicate the presence of a



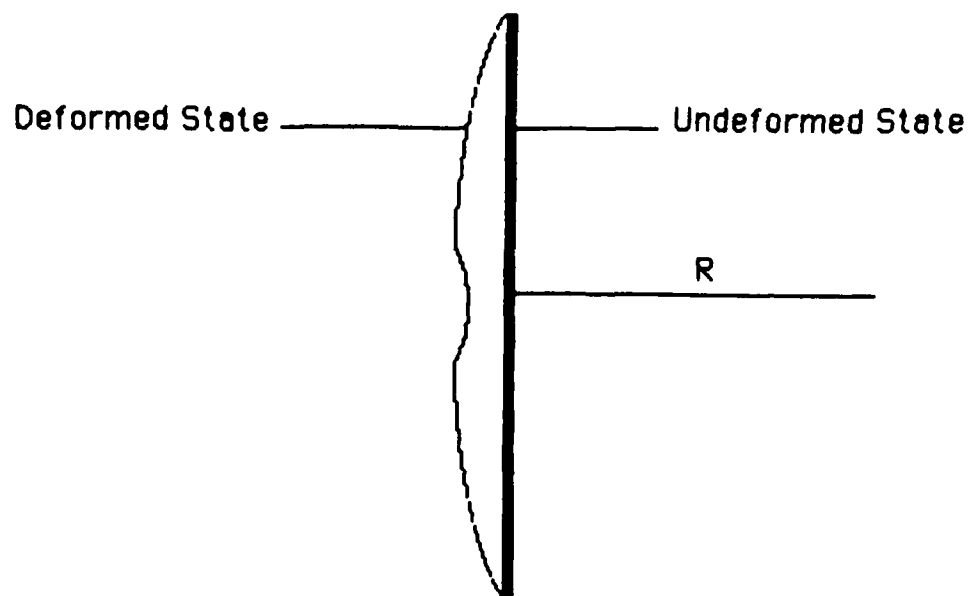


Fig. 25. Panel Deformation as Load is Applied  
(Vertical Plane of Symmetry)

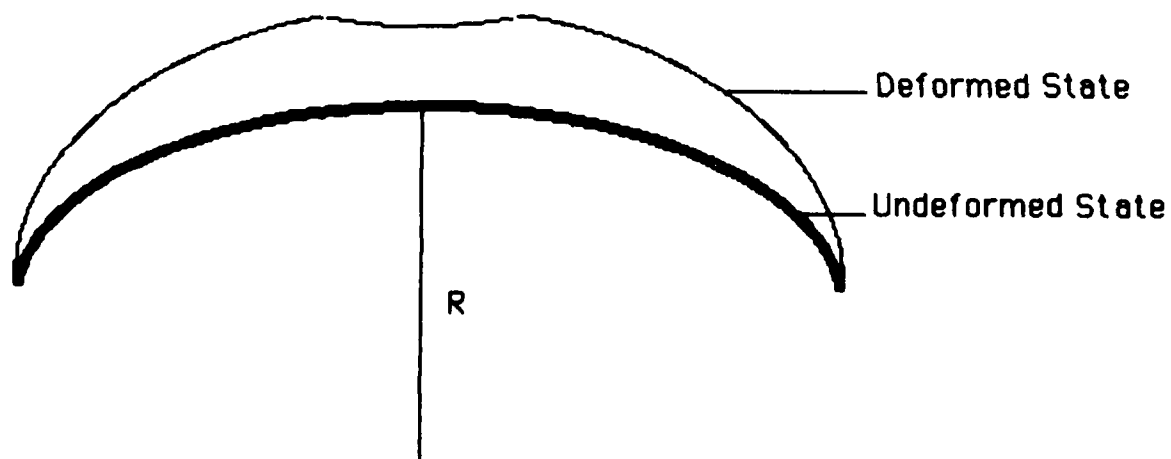


Fig. 26. Panel Deformation as Load is Applied  
(Horizontal Plane of Symmetry)

significant tensile strain on the outside surface or the side opposite the center of curvature of the delaminated layer and a smaller tensile strain on the inside surface. This large tensile strain restrained the delaminated area from snapping out away from the main body of the plate which would require more strain energy. Instead, when the weakened delaminated area buckled locally prior to the global buckling of the panel, it moved toward the center of curvature or the path of least resistance and the smallest strain energy.

When the buckling load for the entire panel is reached, the panel buckles catastrophically. The sides move toward the center of curvature and the center of the panel move away from the center. Fig. 27 shows the horizontal line of symmetry of the panel and the relative movement when the panel buckles. The buckled shape for panel Q122T is shown in Fig. 28. It is interesting to note, that the Q14T panels displayed a snap-through behavior in the buckled state. The four inch delamination extended beyond the center deformation away from the center of curvature (Fig. 29) and subsequently the edges of the delaminated layer are in a state of compression caused by the outer surface bending. This compressive force causes a small local buckle on the outer surface of the delamination (Fig. 29). The buckling patterns for the panels with no delaminations and with total delaminations

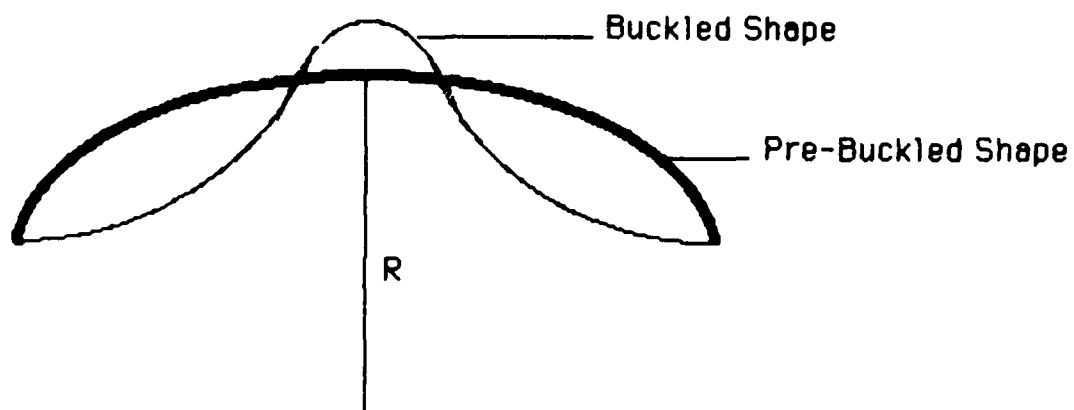


Fig. 27. Panel Buckling Shape (Horizontal Plane of Symmetry)

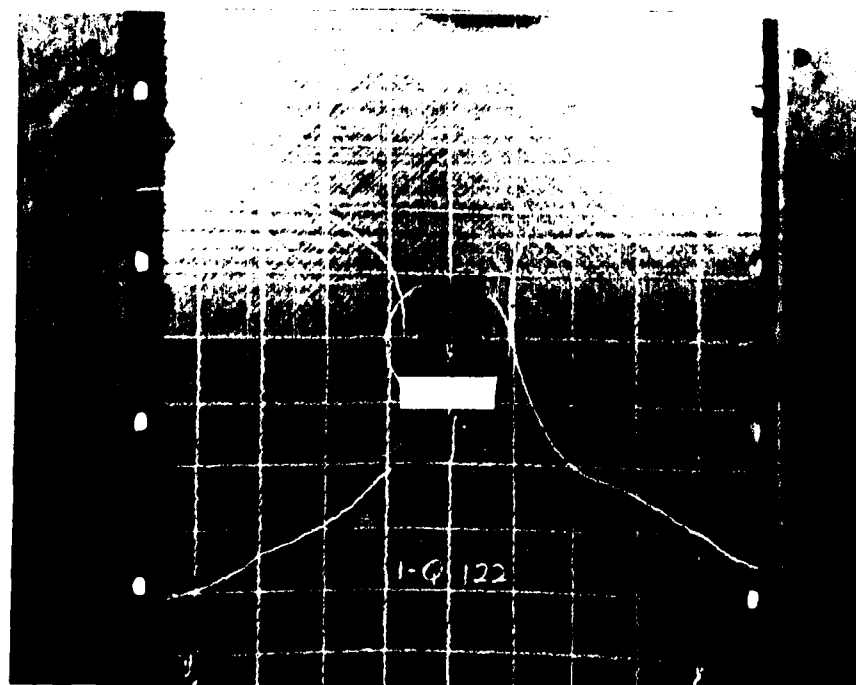


Fig. 28. Q122T in its Buckled Shape



Fig. 29. Local Buckling on the Outer Surface

caused by the teflon inserts are very consistent with the shape of panel Q122T (Fig. 28).

The panels with partial delaminations also displayed much the same type of buckling shape, but with many more exceptions. With these panels, there is a greater tendency toward asymmetrical buckling shapes. Some of these are shown in figures 30 and 31. Earlier work [9,14] found that the position of the 1/4 inch gap in the vertical side supports influenced the buckling shape. This was not the case for these panels since placing the 1/4 inch gap at different positions did not effect the buckling shape. The amount and shape of the delamination appeared to be the determining factor

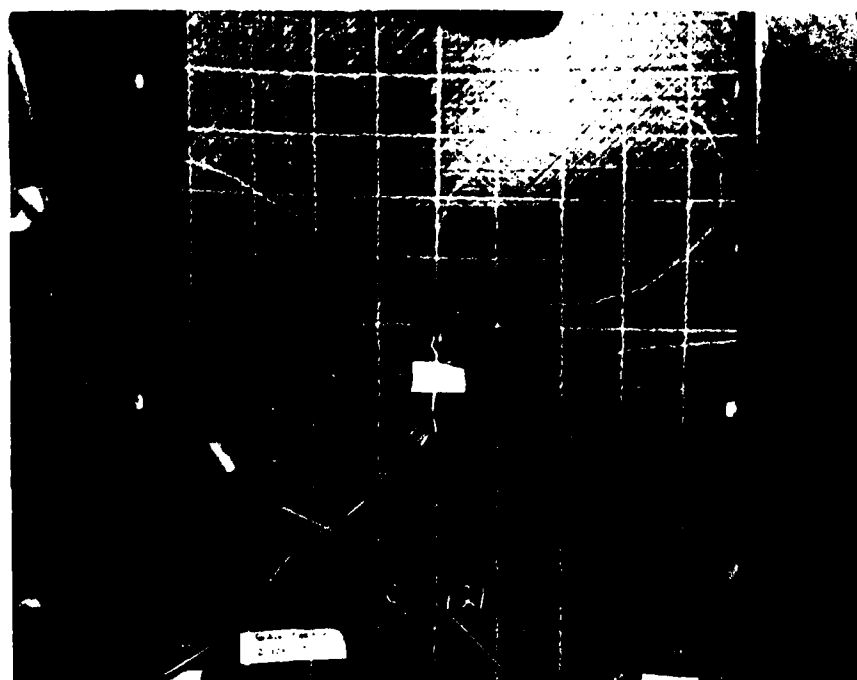


Fig. 30. Asymmetrical Buckling Pattern of Panel Q121

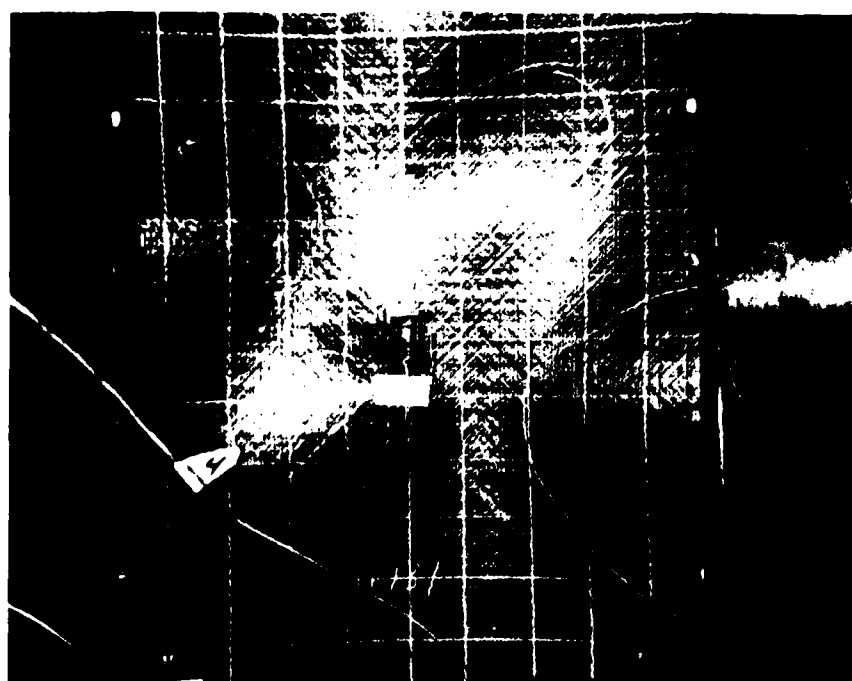


Fig. 31. Asymmetrical Buckling Pattern of Panel Q131

in the symmetry of the buckling shape. This was determined from the panels with the mylar inserts which had their delaminations physically broken free. In several of these panels which had previously buckled in an asymmetrical shape, buckled in the symmetrical shape after the delaminations were broken free. These findings will be discussed in more detail in the Verification Testing section. Also, all the panels which were depled and stereo x-rayed buckled in the symmetrical shape and were subsequently found to have symmetrical delamination areas.

#### X-ray/C-scan Results

The purpose of this research was to determine what effect partial and complete delaminations had on the strength of the composite panels and if they would grow upon buckling. There are several ways to determine delamination growth, two of which are with x-ray pictures and C-scanning. Several of the panels with one delamination were selected to be x-rayed and all 56 of the panels were C-scanned after buckling.

The x-ray procedure involves drilling a 1/4 inch hole in the center of the delamination with a carbide drill. The panel was securely clamped to prevent any vibration which might cause the delamination to grow. A penetrant, tetrabromoethane (TBE), is introduced into the hole and allowed

to diffuse throughout the delaminated area. After the penetrant is allowed to dissipate for approximately 1/2 hour an x-ray is taken. The penetrant in the x-ray will appear darker in the damaged or delaminated area than in the virgin part of the panel (Fig. 32). The circular part of Fig. 32 is completely delaminated. Fig. 33 shows a partial delamination shown by the darkened area. This technique can only be used on the panels with one delamination present since only one-dimensional information can be obtained. Based on the results of the x-rays it was apparent that no delamination growth and very little matrix cracking occurred in the panels with one delamination after they had buckled. Also, these x-rays showed that the panels with the mylar inserts only partially delaminated while the panels with teflon inserts completely delaminated.

Some anomalies were noted in the x-ray process. Figures 34 and 35 are two x-rays of the same panel taken at different times. In Fig. 34 the TBE was allowed 1/2 hour to penetrate the delaminated area, while in Fig. 35 the TBE was given one hour to dissipate. The differences are quite obvious which implies the time dependence of the x-ray results. A period of time longer than an hour was not needed since the TBE diffused to the outer edge of the delamination causing insert. Consequently, one hour is allowed for all the x-rays used in this study.



Fig. 32. X-Ray of Completely Delaminated Panel



Fig. 33. X-Ray of Partially Delaminated Panel





Fig. 34. X-Ray of Q133 After 1/2 Hour Diffusion



Fig. 35. X-Ray of Q133 After One Hour Diffusion

The C-scan results differ significantly from the x-ray results. The C-scan technique transmits sound waves through an object and will detect any difference in the transmissibility of the material. C-scanning has been used successfully to detect delaminations in composite laminates for some time. However, these delaminations were caused by impact or material imperfections [1,2], not from using inserts to cause fabricated delaminations. A comparison of the C-scan and x-ray results for several of the panels using a single mylar insert revealed that the mylar was being detected in the C-scans. This was evident because the x-rays show a much smaller delaminated area than the C-scans do. The C-scans also showed a complete circular delamination (the shape of the insert) where the x-rays showed an irregular shape. However, the C-scans indicated that no delamination growth occurred which was verified by the x-rays.

#### Stereo X-ray

As mentioned, stereo x-ray is used to obtain a 3-D picture of a structure. The results from this procedure are very informative. The 3-D nature of the results do not lend themselves well to depiction on paper, but the results can be shown in a picture showing the amount of delamination present between two plies which is determined from the process. Panel

Q241 (Ref. Table I) was one of the panels stereo x-rayed. Fig. 36 shows how a normal x-ray would appear with the delamination appearing as the dark area. The interpretation of the stereo pair is shown in Fig. 37. The dark area encircled with the dashed line is a delamination between plies six and seven. The remaining delaminated area is between plies five and six. The best angle of incidence,  $\beta$  (Fig. 3), for the x-ray pair is  $\pm 60^\circ$  from the vertical. This angle gives the most separation of the plies with a tolerable level of distortion. The stereo pairs with  $\beta = \pm 15^\circ$  did not provide enough ply separation and therefore, are difficult to interpret.

Due to limited available resources, only six panels were stereo x-rayed. They were Q221, Q323, Q423, Q521, Q232, and Q241. Fig. 38 shows the knockdown factor versus the actual total delaminated area for these panels. Here total delaminated area refers to the area between the plies no longer bonded together without taking into account whether both sides of the teflon or mylar inserts are de-bonded. This data will be discussed further in the Equivalent Delamination section. Appendix D contains the ply-by-ply delaminated area determined through the stereo x-ray technique.

#### Deply Technique

The deply technique was equally effective in displaying the amount of



Fig. 36. Normal X-Ray of Panel Q241



Fig. 37 Interpretation of Stereo X-Ray of Panel Q241

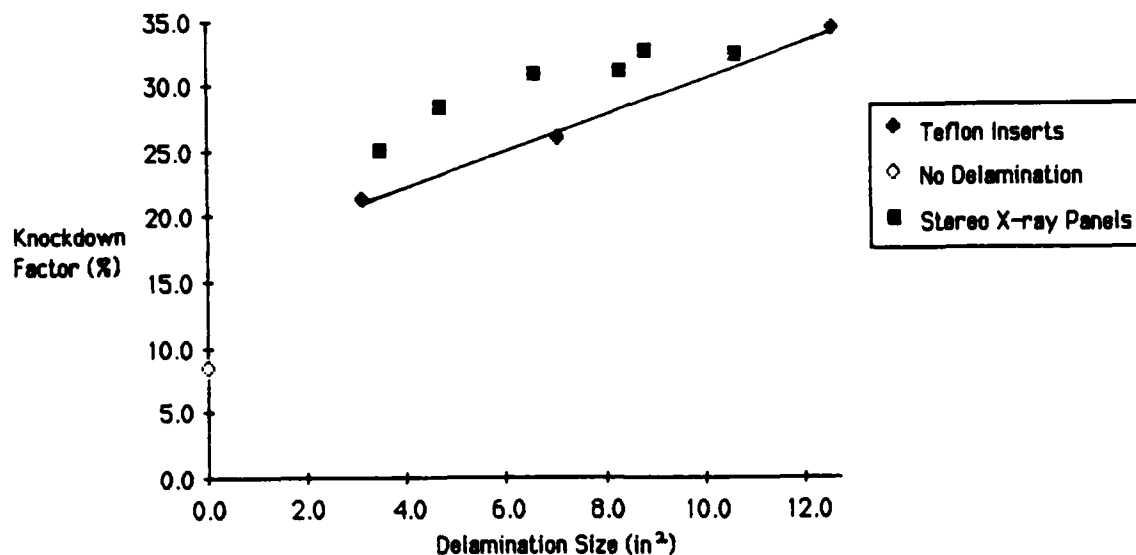


Fig. 38. Knockdown Factor vs Total Actual Delaminated Area at Buckle (Stereo X-Ray Panels)

delamination between individual plies. The technique has to be refined to account for the thickness of the panels and the preset delaminations. The time in the furnace has to be lowered to 50 minutes at 800° F to prevent the plies from completely falling apart upon separation. The time and technique for allowing the gold chloride solution to penetrate the laminate had to be adjusted to better display the gold residue upon deplying. To accomplish this, the gold chloride solution was re-applied every 10 minutes for 1 1/2 hours. This technique ensured that enough gold is present to see without the aid of a microscope. The ply-by-ply results from this technique for panel

Q522 are shown in Fig. 39. The gold indicating a delamination is the light colored substance in the pictures. It is interesting to note that the delaminations located closer to the center of curvature for Q522 contained more gold residue indicating more severe delaminations. Also, these delaminations are better defined and larger which indicates delaminations located toward the inner surface or center of curvature are more critical than delaminations located toward the outer surface. The same indicators were present in Q421.

The other panels deplied include; Q223, Q322, Q421, Q231, Q243, and Q124T. Fig. 40 shows the knockdown factors versus actual total delaminated area for the above panels. This data will be further discussed in the next section. Appendix E contains the delaminated area between the plies for all the panels that were deplied. Interestingly, both the stereo x-ray and deply results for a panel with the same number of mylar inserts results in approximately the same total area. This result is expected since both the panels are from the same large fabricated panel, which is a validation of the results for the two examination techniques.

#### Equivalent Delamination

The results of the deplying and stereo x-ray are used to determine an

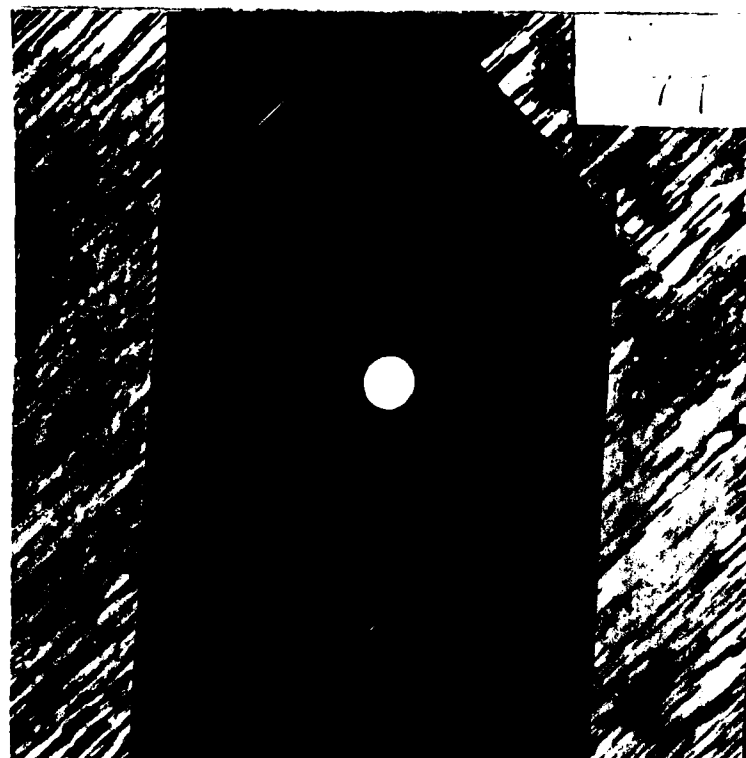


Fig. 39a. Delamination Between Plies Six and Seven ( $-45^{\circ}$  Ply)

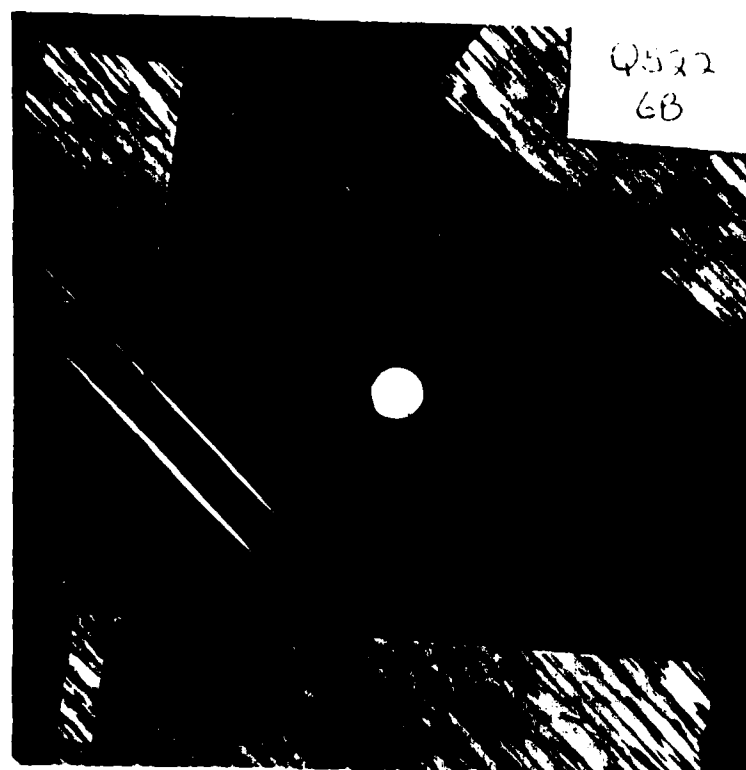


Fig. 39b. Delamination Between Plies Five and Six ( $+45^{\circ}$  Ply)

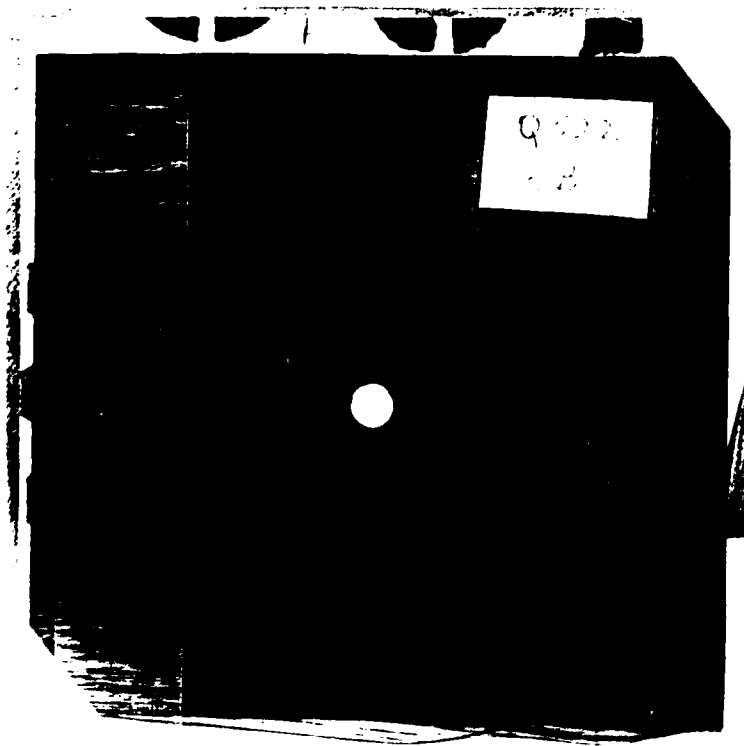


Fig. 39c. Delamination Between Plies Four and Five (  $90^\circ$  Ply)

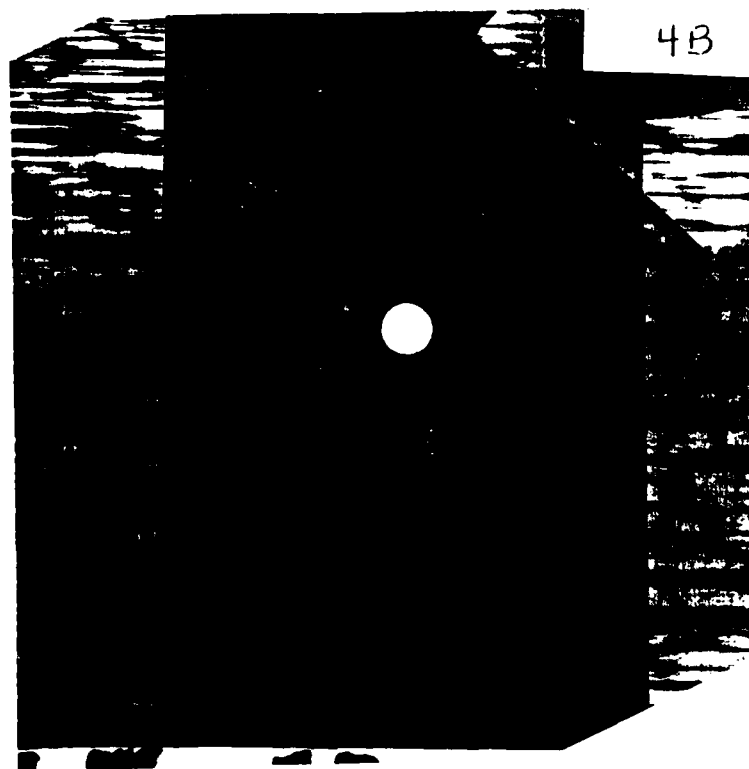


Fig. 39d. Delamination Between Plies Three and Four (  $90^\circ$  Ply)



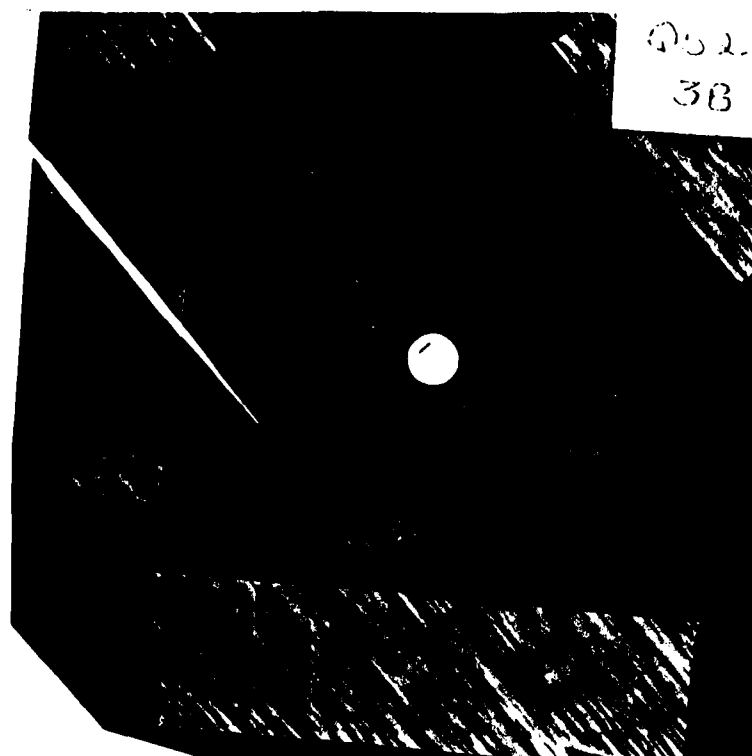


Fig. 39e. Delamination Between Plies Two and Three (+45° Ply)

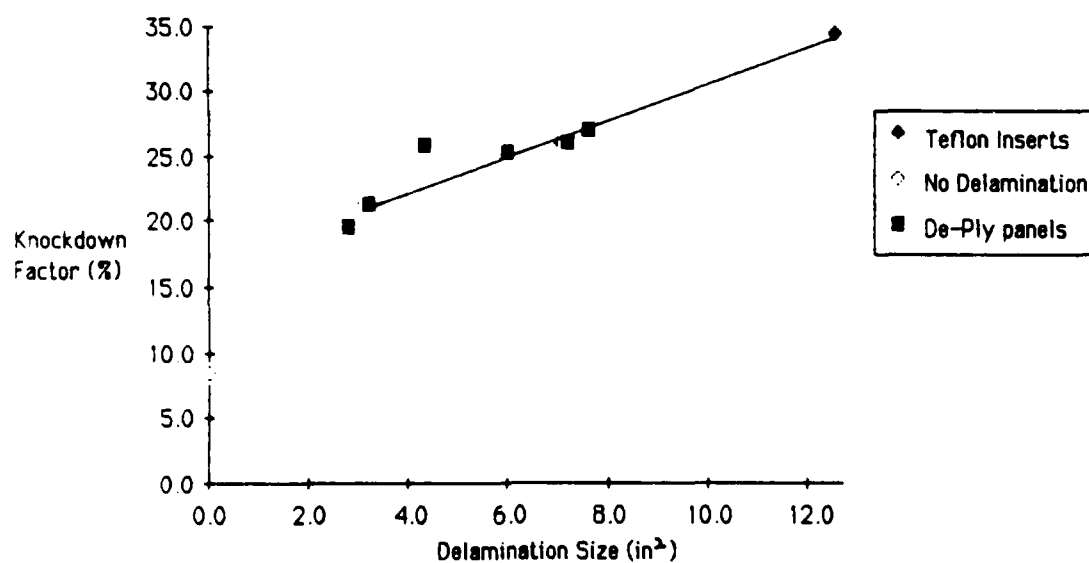


Fig. 40. Knockdown Factor vs Total Actual Delaminated Area at Buckle (De-Ply Panels)

equivalent delamination. Only the 12 panels mentioned earlier are used for this purpose. The total delaminated area for these panels are shown in Table II (See Appendices D and E). Two data points could be used to determine an equivalent delamination, the first being absolute knockdown

<u>Panel</u>	<u>Total Delaminated Area (in<sup>2</sup>)</u>
Q221	3.46
Q223	2.83
Q322	5.97
Q323	4.71
Q421	7.54
Q423	6.60
Q521	8.33
Q522	7.23
Q231	9.54
Q232	10.6
Q241	8.8
Q243	6.28

Table II. Total Delaminated Area In Deply and Stereo X-Ray Panels

factor from the STAGSC-1 buckling load and the second, the experimental end-shortening of the panels.

From earlier findings, Fig. 41 shows a plot of the knockdown factor versus the total delaminated area for the 12 panels. The results of Q12T, Q13T, and Q14T are included again as a reference line for the effect of a

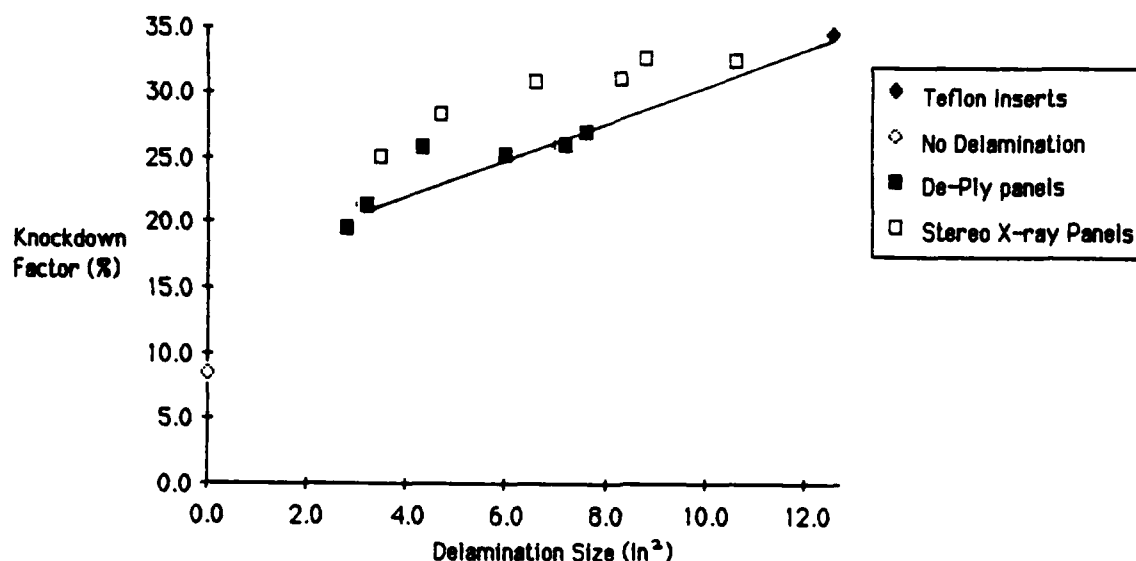


Fig. 41. Knockdown Factor vs Total Actual Delaminated Area (De-Ply and Stereo X-Ray Panels)

single total delamination of a given area. Almost all of the data points lie above the reference line, which indicates that the panels with multiple delamination locations are weaker than the panels with a single delamination for the same delamination area. The difference does not appear to be more than 5 %.

Fig. 42 is a plot of the end-shortening versus total delaminated area. Again the majority of data points lie above the reference line. This indicates that the panels with the centroid of the delaminated area closer to the center of curvature end-shorten more for a given load before buckling.

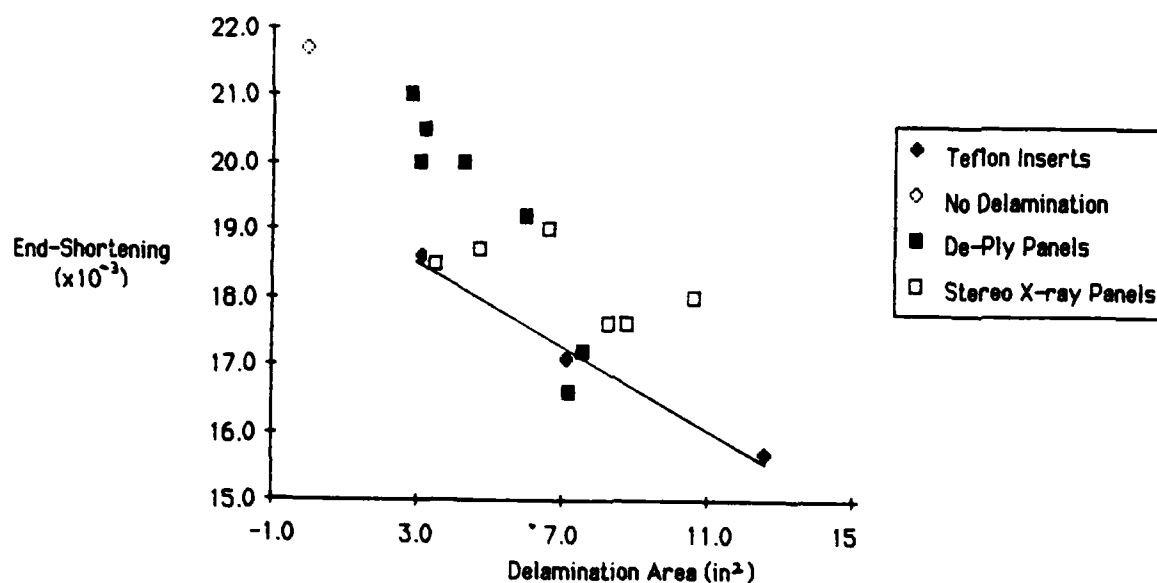


Fig. 42. End-Shortening vs Total Actual Delaminated Area (De-Ply and Stereo X-Ray Panels)

This follows the results of the Q12T and Q12TM panels. Although the knockdown factor was within 0.3 %, the end-shortening of the Q12TM panels is  $20.4 \times 10^{-3}$  in. while the Q12T panels is only  $18.6 \times 10^{-3}$  in.

The data in Fig. 42 also suggest that the panels with multiple delaminations of the same total area as a single delamination are more flexible. However, the panels with multiple delaminations buckle after absorbing less total strain energy than those with a single delamination.

### Verification Testing

In order to verify the experimental results and the amount of delamination present, the delaminations in several of the panels are physically broken free. To accomplish this, the panels are bent opposite their curvatures. This bending action creates compressive bending stresses in the delaminated region which caused the delaminated region to snap-through or buckle locally. By moving the small buckled area around the area of the insert, the delaminated area is known to be totally free. Panels with both teflon and mylar inserts are used for this purpose. They were retested and the results were tabulated.

The panels with the teflon inserts are used more as control panels because the x-rays already show that the delaminations are complete in these panels. It was important to include these panels to ensure that the technique to break the delaminations free did not cause any damage to the panel. The results for the panels with teflon inserts showed no difference in buckling loads greater than  $\pm 2\%$ . The panels with the mylar inserts had their buckling load decrease to approximately the level of the teflon panel results. This was expected since now the mylar panels had a complete delamination of known size.

Several of the panels which buckled in an asymmetrical shape before,

now after the delamination is free, buckled in the normal symmetrical shape mentioned earlier. This indicates the dependance of the buckling mode shape on the size and shape of the delamination.

## V. CONCLUSIONS

The following conclusions can be made based upon this work. These conclusions are separated into two parts. The first with buckling instability and the second with experimental procedures.

### Buckling Instability

1. The total delaminated area effects strength degradation more than delamination location.
2. The buckled shape of the panels influence the delamination snap-through effect. The panels with the two inch delaminations do not experience any outer surface snap-through because of the large tensile force present. The delaminated region in these panels snap-through to a state of the least strain energy which is toward the center of curvature. The three and four inch delaminations experience local buckling of the outer surface resulting from the compressive bending stresses present.
3. Asymmetrical delaminated areas result in asymmetrical buckling patterns. This is verified by the panels which had their delaminations physically broken free, panels which had buckled asymmetrically before buckled symmetrically after the delamination was broken free.

4. The total delaminated area influences the knockdown factor more than the number of delaminations. Although, the closer the delamination is to the center of curvature the larger end-shortening the panel can take at buckling.
5. A delamination located on the inner surface has a greater tendency to grow. The stereo x-ray and de-ply results indicate that these are the locations where the complete delamination of the mylar inserts occurred.
6. Normalizing the experimental buckling loads with respect to thickness using STAGSC-1 results caused the apparent randomness of the buckling loads for the panels with the same delamination location to vanish for the panels with teflon inserts. Thus, panel thickness is an important parameter in the buckling problem.

#### Experimental Procedures

1. There is still a need for a delamination causing insert. The teflon inserts did completely delaminate but, 2 mils is too thick for more than one insert per laminate. A thinner insert is necessary for multiple delaminations.
2. Standardized times and a less toxic penetrant are needed for x-raying composite laminates. The results of the x-ray work indicated the time



dependance of the, tetrabromoethane (TBE) dissipation through the damaged area of the panels.

3. The test fixture provides boundary conditions which are very near those it was designed to provide. The 1/4 inch gap on the vertical sides does not influence the buckling shape of the panels. However, they do need to be centered to give consistent buckling loads.
4. The deply technique and stereo x-ray are both good methods to determine the extent of prefabricated delaminations. The modified techniques of application time for the gold chloride for deply and the  $\pm 60^\circ$  from vertical for stereo x-ray worked well.
5. The C-Scan results can not be relied upon to locate the extent of a delamination if an insert is being used to create the delamination.

### Bibliography

1. Chai, H., Knauss, W. G. and Babcock, C. D., "Observation of Damage Growth in Compressively Loaded Laminates," Experimental Mechanics, Vol. 23, No. 3, p.329, September, 1983.
2. Chai, H., "The growth of Impact Damage in Compressively Loaded Laminates," Ph.D. Thesis, California Institute of Technology, March, 1982.
3. McCarty, J. E. and Ratwani, M. M. Damage Tolerance of Composites: Interim Report, 1 October 1983- 29 February 1984. Contract F33615-82-C-3213. Boeing Military Airplane Company, Seattle Washington, March, 1984.
4. Chai, H., Babcock, C. D., and Knauss, W. G., "One Dimensional Modelling of Failure in Laminated Plates by Delamination Buckling," International Journal of Solids and Structures, Vol. 17, No. 11, pp. 1069-1083, 1981.
5. Simites, G.J., Sallam, S., and Yin, W. L., "Effect of Delamination of Axially Loaded Laminated Plates," AIAA/ASME/ASCE/AHS 25th SDM Conference, Paper 84-0964, May, 1984.
6. Chai, H., and Babcock, C.D., "Two-Dimensional Modeling of Compressive Failure in Delaminated Laminates," Journal of Composite Materials, Vol. 19, pp. 67-98, Jan., 1985.
7. Shivakumar, K. N., and Whitcomb, J. D., "Buckling of a Sublaminates in a Quasi-Isotropic Composite Laminates," Journal of Composite Materials, Vol. 19, pp. 2-18, Jan., 1985.
8. Fei, Z., and Yin, W. L., "Post-buckling Growth of a Circular Delamination in a Laminate Under Compression and Bending," Proceedings of the Southeastern Conference on Theoretical and Applied Mechanics XII, Vol II, 130-134, May, 1984.
9. Seifert, G. R., The Effect of Center Delamination on the Instability of Composite Cylindrical Panels, Masters Thesis, AFIT/GAE/AA/ 84D-25,

Air Force Institute of Technology, WPAFB, Ohio, December, 1984.

10. Wilkins, D. J., "Compression Buckling Tests of Laminated Graphite-Epoxy Curved panels," AIAA Journal, 13: 465-470, April, 1975.
11. Jones, Robert M., Mechanics of Composite Materials, McGraw-Hill, New York, 1975.
12. Almroth, B. O., Brogan, F. A., and Stanley, G. M., Structural Analysis of General Shells. Volume II User instruction for STAGSC-1, Lockheed Palo Alto Research Laboratory, California, January, 1981.
13. Janisse, Thomas C., A Parametric Study of Surface Imperfections and Small Cutouts in a Composite Panel, Masters Thesis, AFIT/GAE/AA/82D-15, Air Force Institute of Technology, WPAFB, Ohio, December, 1982.
14. Hebert, J. S., Analytical/Experimental Linear Bifurcation of Curved Cylindrical Composite Panels, Master's Thesis, AFIT/GAE/AA/83D-14, Air Force Institute of Technology, WPAFB, Ohio, December, 1983.
15. Rummel, W. D., Tedrow, T., and Brinerhoff, H. D., "Enhanced X-ray Stereoscope NDE of Composite Materials," Air Force Wright Aeronautical Laboratories Technical Report AFWAL-TR-80-3053, June, 1980.
16. Sendekyj, G. P., Maddux, G. E., and Porter, E. "Damage Documentation in Composites by Stereo Radiography," Damage in Composite Materials, ASTM STP 775, K. L. Reifsnider, Ed., American Society for Testing and Materials, pp.16-26, 1982.
17. Sendekyj, George P., "NDE Techniques for Composite Laminates," AGARD Specialists' Meeting on Characterization, Analysis and Significance of Defects in Composite Materials, London, UK, 11-14 April, 1983.

18. Freeman, S. M., "Damage Progression in Graphite-Epoxy by Deploying Technique," Air Force Wright Aeronautical Laboratories Technical Report AFWAL-TR-81-3157, December 1981.
19. Garg, A., and Ishai, O., "Hygrothermal Influence on Delamination Behavior of Graphite/Epoxy Laminates," Engineering Fracture Mechanics, Vol. 22, No. 3, pp.413-427, 1985.

## Appendix A

### Stiffness and Effective Laminate Properties

The stiffness matrices for the  $(0/-45/+45/90)_s$  composite laminate are given below for the material properties of the AS4/3501-6 graphite/epoxy used in this thesis. The coupling stiffness matrix  $[B_{ij}]$  for this quasi-isotropic laminate is equal to zero due to the symmetrical layup. Due to the large variations in thickness of the experimental panels, the matrices for three different thicknesses are included for comparison. The three thicknesses include; the minimum, median, and the maximum. The matrices are:

for  $t = 0.0384$

#### Extensional Stiffness

$$A_{ij} = \begin{bmatrix} 0.3157 & 0.0925 & 0.0 \\ 0.0925 & 0.3157 & 0.0 \\ 0.0 & 0.0 & 0.1116 \end{bmatrix} \times 10^6 \text{ lb/in}$$

Bending Stiffness

$$D_{ij} = \begin{bmatrix} 63.765 & 9.605 & -3.867 \\ 9.605 & 17.362 & -3.867 \\ -3.867 & -3.867 & 11.947 \end{bmatrix} \quad \text{lb}$$

for  $t = 0.0390$

Extensional Stiffness

$$A_{ij} = \begin{bmatrix} 0.3207 & 0.0940 & 0.0 \\ 0.0940 & 0.3207 & 0.0 \\ 0.0 & 0.0 & 0.1133 \end{bmatrix} \quad \times 10^6 \text{ lb/in}$$

Bending Stiffness

$$D_{ij} = \begin{bmatrix} 66.800 & 10.062 & -4.051 \\ 10.062 & 18.188 & -4.051 \\ -4.051 & -4.051 & 12.516 \end{bmatrix} \quad \text{lb}$$

for  $t = 0.0408$

Extensional Stiffness

$$A_{ij} = \begin{bmatrix} 0.3355 & 0.0983 & 0.0 \\ 0.0983 & 0.3355 & 0.0 \\ 0.0 & 0.0 & 0.1186 \end{bmatrix} \times 10^6 \text{ lb/in}$$

Bending Stiffness

$$D_{ij} = \begin{bmatrix} 76.483 & 11.521 & -4.638 \\ 11.521 & 20.825 & -4.638 \\ -4.638 & -4.638 & 14.330 \end{bmatrix} \text{ lb}$$

Effective Laminate Properties [11]

Longitudinal Youngs' Modulus:  $E_x = (A_{11}A_{22} - A_{12}^2) / tA_{22} = 7.516 \times 10^6$

Transverse Youngs' Modulus:  $E_y = (A_{11}A_{22} - A_{12}^2) / tA_{11} = 7.516 \times 10^6$

Longitudinal Poissons' Ratio:  $\nu_{xy} = A_{12} / A_{22} = 0.293$

These effective laminate properties are used in the calculations in

Appendix B.

## Appendix B

### Analytical Non-Dimensionalized Values

The panels with the teflon inserts are used to determine if snap-through or delamination growth will occur. These panels were chosen because they represent worst case since total delaminations are present. The panels evaluated included; Q123T, Q134T, and Q144T. These panels were instrumented with back to back strain gage rosettes located at the delamination center. The data used in Equations (13), (14), and (15) are taken from the strain gage readings, orientated in the x direction, when the front and back gages begin reading differently during the test. This behavior indicates the onset of the snap-through phenomenon. Recalling Equations (13), (14), and (15):

$$\rho = \mu h / 2\epsilon \quad (13)$$

$$\tilde{a} = [12(1-\nu^2)\epsilon]^{1/2} a/h \quad (14)$$

$$\tilde{G} \tilde{a}^4 = [12(1-\nu^2)]^2 G^* a^4 / Eh^5 \quad (15)$$



Equation (15) indicates a need for the fracture toughness,  $G^*$ , of AS4/3501-6 graphite/epoxy.  $G^*$  for dry 3501-6 graphite/epoxy is 0.7423 in-lbs/in<sup>2</sup> [19]. Equation (13) is not used in this analysis since actual strain measurements are available. Since  $\rho$  represents the ratio of bending strain vs the membrane strain, a weighted average of the front and back strain gage readings represents the compressive membrane strain for the panel. The difference between this average and the strain value on the surface of the delamination is the strain due to bending. The ratio,  $\rho$ , is simply this difference divided by the average strain. This procedure is shown for panel Q123T below.

Recalling the results from Appendix A:

$$\nu_{xy} = 0.293$$

$$E_x = 7.516 \times 10^6 \text{ psi}$$

#### Panel Q123T

$$\epsilon_{\text{front}} = -320 \times 10^{-6} \text{ in/in} \quad \epsilon_{\text{back}} = -200 \times 10^{-6} \text{ in/in}$$

$$a = 1 \text{ in,}$$

$$h=0.0098$$

$$\epsilon_{\text{mem}} = [6/8(-320 \times 10^{-6}) + 2/8(-200 \times 10^{-6})]$$

$$\epsilon_{\text{mem}} = -290 \times 10^{-6} \text{ in/in}$$

$$\rho = -290 \times 10^{-6} - (-200 \times 10^{-6}) / -290 \times 10^{-6}$$

$$\rho = 0.310$$

$$\tilde{a} = [12(1 - 0.293^2) 290 \times 10^{-6}]^{1/2} [1/0.0098]$$

$$\tilde{a} = 5.76$$

$$\tilde{G} \tilde{a}^4 = [12(1 - 0.293^2)]^2 (0.7423)(1^4) / (7.516 \times 10^6)(0.0098^5)$$

$$\tilde{G} \tilde{a}^4 = 1.31 \times 10^5$$

#### Panel Q134T

$$\epsilon_{\text{front}} = -420 \times 10^{-6} \text{ in/in} \quad \epsilon_{\text{back}} = -600 \times 10^{-6} \text{ in/in}$$

$$a = 1.5 \text{ in}$$

$$h = 0.00965$$

$$\epsilon_{\text{mem}} = -465 \times 10^{-6}$$

$$\rho = 0.290$$

$$\tilde{a} = 11.10$$

$$\tilde{G} \tilde{a}^4 = 7.180 \times 10^5$$

#### Panel Q144T

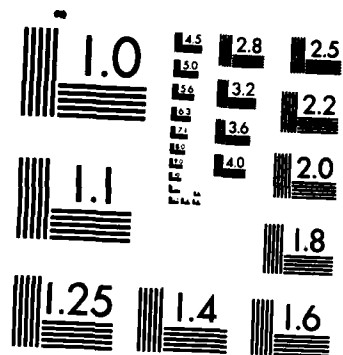
$$\epsilon_{\text{front}} = -490 \times 10^{-6} \text{ in/in} \quad \epsilon_{\text{back}} = -440 \times 10^{-6} \text{ in/in}$$

$$a = 2.0 \text{ in}$$

$$h = 0.009825$$

AD-A164 110 THE EFFECTS OF THROUGH THE THICKNESS DELAMINATIONS ON 2/2  
CURVED COMPOSITE PANELS(U) AIR FORCE INST OF TECH  
WRIGHT-PATTERSON AFB OH SCHOOL OF ENGI B A HORBAN  
UNCLASSIFIED DEC 85 AFIT/GAE/AA/85D-8 F/G 13/13 NL





MICROCOPY RESOLUTION TEST CHART  
NATIONAL BUREAU OF STANDARDS-1963-A

$$\epsilon_{\text{mem}} = -477.5 \times 10^{-6}$$

$$\rho = 0.079$$

$$\tilde{a} = 14.73$$

$$\tilde{G} \tilde{a}^4 = 20.77 \times 10^5$$

An extrapolation of the table given by Fei and Yin [8] indicates that for snap-through to occur, based on the value calculated for  $\rho$ ,  $\tilde{a}$  must be larger than 5.67, 5.53, and 3.93, respectively for panels Q123T, Q134T, and Q144T. The values calculated for  $\tilde{G} \tilde{a}^4$  indicate that delamination growth will not occur since the calculated values are 100 times larger than the minimum value needed for growth to occur. These findings, delamination snap-through will occur and no delamination growth, were experimentally verified.

## Appendix C

### Test Data

The raw test data for the panels are included in this appendix. The individual small groups are for each delamination type panel. The various columns represent:

Panel - panel number

h - average panel thickness (in)

STAGC-1 - calculated STAGSC-1 buckling load for panel thickness (lbs)

Exper. - Experimentally determined buckling load (lbs)

KDF - Knockdown factor from STAGSC-1 panel buckling load (%)

Deflection - Experimentally determined panel end-shortening ( $\times 10^{-3}$  in)

Panel	h	STAGC-1	Exper.	KDF	Deflection
Q002	.0384	4848.9	4487	7.5	22.6
Q003	.0389	4980.8	4589	7.9	23.6
Q004	.0386	4901.7	4431	9.6	19.0
Q122	.0384	4848.9	3684	24.0	17.0
Q123	.0389	4980.8	4005	19.6	21.5
Q124	.0384	4848.9	3610	25.6	19.8
Q121T	.0391	5033.9	3861	23.3	15.2
Q122T	.0390	5007.3	3992	20.3	19.2
Q123T	.0392	5060.5	3977	21.4	18.0
Q124T	.0392	5060.5	4040	20.2	22.0

Panel	h	STAGC-1	Exper.	KDF	Deflection
Q131	.0387	4928.0	4030	18.2	22.0
Q133	.0389	4980.8	3750	24.7	21.6
Q134	.0399	5248.4	4257	18.9	20.6
Q131T	.0388	4954.4	3702	25.3	17.0
Q132T	.0385	4875.3	3614	25.9	17.5
Q133T	.0386	4901.7	3779	25.4	17.6
Q134T	.0386	4901.7	3566	27.2	16.4
Q141	.0388	4954.4	2980	39.8	16.2
Q142	.0388	4954.4	3160	36.3	17.6
Q143	.0386	4901.7	2980	39.2	15.2
Q144	.0386	4901.7	3787	22.7	14.2
Q141T	.0391	5033.9	3236	35.7	14.0
Q144T	.0393	5087.2	3498	33.0	17.4
Q122TM	.0397	5194.5	4066	21.7	20.9
Q124TM	.0395	5140.8	4099	20.3	20.0
Q221	.0384	4848.9	3639	25.0	18.5
Q222	.0385	4875.3	4004	17.9	20.0
Q223	.0386	4901.7	3947	19.5	21.0
Q224	.0388	4954.4	4677	5.6	24.8
Q321	.0397	5194.5	4202	19.1	19.0
Q322	.0396	5167.6	3867	25.2	19.2
Q323	.0394	5113.9	3672	28.2	18.7
Q324	.0389	4980.8	3956	20.6	23.2
Q421	.0399	5248.4	3836	26.9	17.2
Q422	.0395	5140.8	4029	21.6	19.4
Q423	.0395	5140.8	3554	30.9	19.0
Q424	.0393	5087.2	3575	29.7	20.0
Q521	.0398	5221.4	3596	31.1	17.6
Q522	.0392	5060.5	3747	26.0	16.6
Q523	.0408	5493.6	4185	23.8	17.1
Q524	.0398	5221.4	3955	24.3	21.0

<u>Panel</u>	<u>h</u>	<u>STAGC-1</u>	<u>Exper.</u>	<u>KDF</u>	<u>Deflection</u>
Q231	.0395	5140.8	3821	25.7	20.0
Q232	.0396	5167.6	3495	32.4	18.0
Q233	.0390	5007.3	4080	18.5	24.0
Q234	.0394	5113.9	3956	22.6	20.8
Q241	.0391	5033.9	3400	32.5	17.6
Q242	.0389	4980.8	3925	21.2	21.4
Q243	.0388	4954.4	3902	21.2	20.5
Q244	.0387	4928.0	4025	18.3	19.8



## Appendix D

### Actual Delaminated Area for Stereo X-ray Panels

The actual delaminated area was determined by studying the stereo pair for each of the panels through a stereoscope. The best way to report the actual delaminated area is with a percent delaminated area. This percent is converted to area by multiplying it by the area of the delamination causing insert. The table below shows which panel is being considered across the top. The left side indicates the plies the delamination is between. The first of the two values in the box, is the percent delaminated area and the second is the corresponding actual area (in<sup>2</sup>). The last row is the total areas for the panels or simply the sum of the column above it. The results are given below:

	Q221	Q323	Q423	Q521	Q232	Q241
6 - 7	25/0.8	30/0.9	10/0.3	30/0.9	70/4.9	30/3.8
5 - 6	85/2.7	40/1.3	30/0.9	15/0.5	80/5.7	40/5.0
4 - 5		80/2.5	80/2.6	25/0.8		
3 - 4			90/2.8	95/3.0		
2 - 3				100/3.1		
Total	3.5	4.7	6.6	8.3	10.6	8.8

## Appendix E

### Actual Delaminated Area for Deply Panels

The actual delaminated area was determined by studying each individual ply for each of the panels. The best way to report the actual delaminated area is with a percent delaminated area. This percent is converted to area by multiplying it by the area of the delamination causing insert. The table below shows which panel is being considered across the top. The left side indicates the plies the delamination is between. The first of the two values in the box, is the percent delaminated area and the second is the corresponding actual area (in<sup>2</sup>). The last row is the total areas for the panels or simply the sum of the column above it. The results are given below:

	Q223	Q322	Q421	Q522	Q231	Q243	Q124T
6 - 7	0/0.0	60/1.9	40/1.3	10/0.3	75/5.3	10/1.3	100/3.1
5 - 6	90/2.8	40/1.3	40/1.3	30/0.9	60/4.2	40/5.0	
4 - 5		90/2.8	60/1.9	40/1.3			
3 - 4			100/3.1	55/1.7			
2 - 3				95/3.0			
Total	2.8	6.0	7.6	7.2	9.5	6.3	3.1

## VITA

Blaise A. Horban was born on 6 February 1959 in Rochester, Indiana. He graduated from Rochester Community High School in 1977 and entered the United States Air Force Academy where he received a Bachelor of Science Degree in Engineering Mechanics and his commission in 1981. He was stationed at Wright Patterson AFB, OH as a Propulsion Performance Engineer on the Advanced Cruise Missile Engine. In 1984 he was accepted into the graduate Aeronautical Engineering program at the AFIT School of Engineering.

Permanent address: R. R. #3 Box 57

Rochester, IN 46975

UNCLASSIFIED

SECURITY CLASSIFICATION OF THIS PAGE

## REPORT DOCUMENTATION PAGE

1a. REPORT SECURITY CLASSIFICATION <b>UNCLASSIFIED</b>			1b. RESTRICTIVE MARKINGS		
2a. SECURITY CLASSIFICATION AUTHORITY			3. DISTRIBUTION/AVAILABILITY OF REPORT <b>Approved for public release; distribution unlimited.</b>		
2b. DECLASSIFICATION/DOWNGRADING SCHEDULE					
4. PERFORMING ORGANIZATION REPORT NUMBER(S) <b>AFIT/GAE/AA/85D-8</b>			5. MONITORING ORGANIZATION REPORT NUMBER(S)		
6a. NAME OF PERFORMING ORGANIZATION <b>School of Engineering</b>		6b. OFFICE SYMBOL (If applicable) <b>AFIT/EN</b>		7a. NAME OF MONITORING ORGANIZATION	
6c. ADDRESS (City, State and ZIP Code) <b>Air Force Institute of Technology Wright-Patterson AFB, Ohio 45433</b>				7b. ADDRESS (City, State and ZIP Code)	
8a. NAME OF FUNDING/SPONSORING ORGANIZATION		8b. OFFICE SYMBOL (If applicable)		9. PROCUREMENT INSTRUMENT IDENTIFICATION NUMBER	
8c. ADDRESS (City, State and ZIP Code)				10. SOURCE OF FUNDING NOS.	
11. TITLE (Include Security Classification) <b>See Box 19</b>				PROGRAM ELEMENT NO.	
				PROJECT NO.	
				TASK NO.	
				WORK UNIT NO.	
12. PERSONAL AUTHOR(S) <b>Blaise A. Horban, M.S., Capt., USAF</b>					
13a. TYPE OF REPORT <b>MS Thesis</b>		13b. TIME COVERED FROM _____ TO _____		14. DATE OF REPORT (Yr., Mo., Day) <b>1985 December</b>	
15. PAGE COUNT <b>102</b>					
16. SUPPLEMENTARY NOTATION					
fr back					
17. COSATI CODES			18. SUBJECT TERMS (Continue on reverse if necessary and identify by block number)		
FIELD	GROUP	SUB. GR.	Composites, Cylindrical Panels, Though the Thickness Delaminations, Experimental Shell Analysis, Finite Elements, STAGSC-1, (Theses).		
11	04				
19. ABSTRACT (Continue on reverse if necessary and identify by block number)					
11) Title: THE EFFECTS OF THROUGH THE THICKNESS DELAMINATIONS ON CURVED COMPOSITE PANELS					
Thesis Advisor: Dr. Anthony N. Palazotto					
<div style="text-align: right;"> <b>Approved for public release 1AW AFB 1985/</b>  <b>LYNN E. WOLAVER 16 UNCL 86</b>  <b>Dean for Research and Professional Development</b>  <b>Air Force Institute of Technology (AFIT)</b>  <b>Wright-Patterson AFB OH 45433</b> </div>					
20. DISTRIBUTION/AVAILABILITY OF ABSTRACT UNCLASSIFIED/UNLIMITED <input checked="" type="checkbox"/> SAME AS RPT. <input type="checkbox"/> DTIC USERS <input type="checkbox"/>			21. ABSTRACT SECURITY CLASSIFICATION <b>UNCLASSIFIED</b>		
22a. NAME OF RESPONSIBLE INDIVIDUAL <b>Dr. Anthony N. Palazotto</b>			22b. TELEPHONE NUMBER (Include Area Code) <b>(513) 255-3517</b>		22c. OFFICE SYMBOL <b>AFIT/EN</b>

DD FORM 1473, 83 APR

EDITION OF 1 JAN 73 IS OBSOLETE.

UNCLASSIFIED  
SECURITY CLASSIFICATION OF THIS PAGE

UNCLASSIFIED

SECURITY CLASSIFICATION OF THIS PAGE

The buckling loads of 8-ply AS4/3501-6 graphite/epoxy delaminated cylindrical panels were determined experimentally. The delaminations fabricated into the laminate, with mylar and teflon inserts, were indicative of low velocity projectile impact damage. The mylar and teflon inserts caused partial and total delaminations, respectively. Two types of delaminations were used; namely, eccentric, off mid-surface, and mid-surface. The eccentric delaminations were placed progressively through the thickness of the laminate. STAGSC-1 finite element computer code results for undelaminated composite panels were compared to the experimental results to obtain a percent strength degradation.

The experimental testing was accomplished by the Air Force Flight Dynamics Laboratory. The test device provided boundary conditions of clamped top and bottom edges and simply supported vertical sides.

Two destructive techniques, stereo x-ray and deply, were used to determine the total delaminated areas and locations. Based in part on these results, one equivalent delamination was obtained corresponding to the total area of the multiple partial delaminations. The panels with multiple delaminations were found to be approximately 5 % weaker than a single delaminated area of the same total size.

Keywords:

FCD 18

UNCLASSIFIED

SECURITY CLASSIFICATION OF THIS PAGE

END

FILMED

3 - 86

DTIC